The Role of Mcl-1 in Developmental Neurogenesis

Sarah Patricia Connolly, B.Sc (Honours)

A thesis submitted to the School of Graduate Studies in partial fulfillment of

the requirements for the degree of

Master of Science in Medicine

(Neuroscience)

BioMedical Sciences

Faculty of Medicine

February 2023

Memorial University of Newfoundland

St. John’s Newfoundland and Labrador

Abstract

Neurogenesis is marked by cell cycle exit and differentiation of neural stem cells (NSCs) into post mitotic neurons. Mitochondrial morphology and function regulate neurogenesis through mediating a metabolic switch from glycolysis to oxidative phosphorylation (OXPHOS). Myeloid cell leukemia 1 (Mcl-1), a member of the B-cell lymphoma 2 family of proteins, is essential for survival of neural precursor cells (NPCs) during neurogenesis. Mcl-1 also regulates mitochondrial dynamics. Currently it remains elusive whether Mcl-1 maintains mitochondrial dynamics during neurogenesis. Therefore, my **hypothesis** is that Mcl-1 promotes survival of NPCs during neurogenesis through mediating mitochondrial dynamics. Conditional knockout mouse lines of Mcl-1 (MKO) were generated using the Cre/Lox system. The effect of Mcl-1 on cell cycle exit in the developing forebrain was determined through a BrdU/EdU pulse assay. Mitochondrial number and morphology in MKO embryos were examined in the medial ganglionic eminence (MGE) through immunohistochemistry (IHC) and electron microscopy (EM). Loss of Mcl-1 resulted in a significantly greater number of NPCs exiting the cell cycle at E11. IHC and EM analysis reveal that mitochondria were more numerous in MKO NPCs. The results of this study suggest that Mcl-1 serves additional roles in mitochondrial dynamics and cell cycle exit during neurogenesis, which may be essential for proper nervous system development.

General Summary

Neurogenesis is the process in which neurons, the primary cell type of the brain, are formed from stem cells. Neurogenesis is mediated by functional and shape changes of mitochondria. A protein known as Mcl-1 is necessary for the survival of stem cells during the period of neurogenesis. Mcl-1 also regulates cell cycle exit and mitochondrial shape changes. However, it is unknown whether Mcl-1 performs these functions during neurogenesis. This thesis aims to determine if Mcl-1 promotes cell cycle exit and mitochondria shape changes during neurogenesis. Loss of Mcl-1 resulted in premature cell cycle exit and subsequent cell death of stem cells at the beginning of neurogenesis. Loss of Mcl-1 results in more mitochondria in stem cells at the beginning of neurogenesis. Taken together these results demonstrate that Mcl-1 is necessary during neurogenesis to mediate cell cycle exit and mitochondrial number, which may be essential for brain development.

Co-authorship Statement

I am the primary contributor to the thesis, but acknowledgment is due to my fellow researchers. The Tom20/Nestin IHC experiment with NanoJ SRRF processing, as described in section 2.8, was developed in collaboration with Dr. Matthew Parsons and Jessica Barron. Processing of tissue and image acquisition for the EM experiments, described in section 2.9, were performed by Nicholas Newhook from Memorial University of Newfoundland's Medical Laboratories Electron Microscopy/ Flow Cytometry/ Confocal Microscopy unit. All other experiments in the thesis were conducted by me.

Acknowledgment

I would like to thank my supervisor Dr. Jacqueline Vanderluit for her immense support and guidance throughout the completion of my graduate degree. It would not have been possible to have completed this thesis without her leadership and advocacy, which has allowed me to prosper personally and professionally. I thank my fellow lab members, past and present, who I have had the privilege of working with throughout my graduate degree.

I would like to thank my committee members Dr. Matthew Parsons and Dr. Craig Moore for their support and guidance throughout my degree, and for their thoughtful insights which helped shaped the experiments of this thesis.

I would like to extend gratitude to all members of the Parsons lab, especially Dr. Matthew Parsons and Jessica Barron, for their collaboration and assistance with the Nestin/Tom20 experiments of my thesis. A special thank you to Stephanie Tucker and Nicholas Newhook of Memorial University's Medical Laboratories-Electron Microscopy/ Flow Cytometry/ Confocal Microscopy unit for all of their assistance with the EM analysis of my thesis.

I would like to acknowledge the Natural Sciences and Engineering Research Council and the Faculty of Medicine of Memorial University for funding of my thesis.

Lastly, I would like to extend gratitude to my family and friends who have supported me through completion of this degree. To my aunts, Anne, Mary, Dorothy and Carmel, for always supporting me. To my best friends William and Josh, for their assistance and encouragement. A special thank you to Shaykat Saha, for assistance at multiple stages of this thesis and for his support throughout. Lastly, to my parents, Patricia and Edward, and my sister, Caitlin. Without their constant support, encouragement and assistance this thesis would not have been possible.

Table of Contents

List of Figures

List of Tables

List of Abbreviations and Symbols

°C – degrees Celsius

% – percent

µg – micrograms

µl – microlitre

µm – micrometer

µM – micromolar

1X – one times

1X HBSS – 1X Hanks' Balanced Salt Solution

A1 – Bcl-2-related protein A1

AC3 – active Caspase 3

APAF 1 – Apoptotic protease activating factor 1

ATP – Adenosine triphosphate

Bad – Bcl-2 associated death promotor

Bak – Bcl-2 homologous antagonist killer

Bax – Bcl-2-associated X protein

baxN– Bax Null

$bax^{f/f}$ – Bax Floxed

Bcl-2 – B cell lymphoma-2

Bcl-w – Bcl-2-like protein 2

Bcl-XL – B-cell lymphoma-extra large

BH – Bcl-2 homology

Bid – BH3 interacting death domain agonist

Bik – Bcl-2 interacting killer

Bim – Bcl-2 interacting mediator of cell death

Bmf – Bcl-2-modifying factor

BP – base pair

BPB – bromophenol blue

BrdU - bromodeoxyuridine

Ca^{2+} - calcium

CARD – Caspase-recruitment domains

CNS – Central nervous system

$Cre^{+/-}$ – nestin mediated cre

Ctl – control

Cux1+ - Cut like homeobox 1

DNA – deoxyribonucleic acid

dNTP – deoxynucleoside triphosphate

Drp-1 – dynamin related protein-1

E – Embryonic day

EdU - 5-ethynl-2'-deoxyuridine

EDTA – Ethylenediaminetetraacetic acid

EtOH - ethanol

FIJI – Fiji is just ImageJ

FOR - forward

H - Hour

H2O – water

HCL- hydrochloric acid

HET – heterozygous

Hrk – Harakiri Bcl-2 interacting protein

IMM – inner mitochondrial membrane

KO – conditional knockout

Lhx5 - LIM homeobox protein 5

Matrix – mitochondrial matrix

Mcl-1 – Myeloid cell leukemia-1

MKO – Mcl-1 conditional knock-out

MKO:Bax KO – Mcl-1 conditional knock-out: Bax conditional knockout

mcl-1 (f/f) – mcl-1 floxed

mg – milligram

min – minute

MFN1 – mitofusion 1

MFN2- mitofusion 2

ml – millilitre

mM – millimolar

MOMP – Mitochondrial outer membrane permeabilization

NKx2.1 - NK2 Homeobox 1

nm – nanometer

nM – nanomolar

NPCs – Neural precursor cells

NRF2 - nuclear factor erythroid 2-related factor 2

NSCs – neural stem cells

OM – outer mitochondrial membrane

Opa-1 - Opa1 mitochondrial dynamin like GTPase

OXPHOS – oxidative phospholylation

PBS – phosphate buffer saline

PCR – polymerase chain reaction

pH – power of hydrogen

PNS – peripherial nervous system

PUMA – P53 upregulated modulator of apoptosis

REV - reverse

ROS – reactive oxygen species

SD – standard deviation

SIM - SIM BHLH transcription factor 1

SRRF – Super resolution radial fluctuations

SRY – sex determining region Y gene

TAE – Tris-acetate EDTA

UV – ultraviolet

VZ – ventricular zone

V – volts

v/v – volume per volume

w/v – weight per volume

Chapter 1: Introduction

1.1 Neurogenesis

Neurogenesis is the process by which new neurons are generated from neural stem cells (NSCs). Though neurogenesis has traditionally believed to occur solely during development, studies have demonstrated that neurogenesis occurs throughout life in two regions of the mammalian central nervous system (CNS); the subventricular zone of the lateral ventricles and the subgranular zone of the dentate gyrus in the hippocampus (Altman & Das, 1965; Reynolds & Weiss, 1992). During embryonic development, NSCs give rise to neurons of the mammalian CNS (Götz et al., 2016). Neurogenesis is a complex process, in which epigenetic mechanisms mediate responses to extracellular cues to determine the expression of regulators of proliferation, fate specification, and differentiation (Yao et al., 2016). Developmental neurogenesis ultimately establishes the neural organization of the CNS (Yao et al., 2016).

1.1.1 Nervous system development and neurogenesis in murine models

Neurulation in mice begins at embryonic day (E) 7.5 of gestation (Angevine & Sidman, 1961; Nornes & Carry, 1978). The nervous system arises from the ectoderm. After gastrulation, neuroepithelial stem cells are induced by signals arising from the mesoderm to change shape and form the neural plate. The neural tube forms from a thickening of the ectoderm known as the neural plate. After the neural tube closes at E10, neuroepithelial stem cells remain within the ventricular zone (VZ) (Anthony et al., 2004). This ultimately establishes a distinct region containing progenitor cells. Proliferation of neuroepithelial

stem cells occurs along the length of the neural tube, and subsequent folding of the neural tube establishes the three brain regions, the developing hindbrain, midbrain, and forebrain. Neurogenesis begins after the formation of the neural tube.

Neurogenesis begins at embryonic day E10 in the spinal cord and hindbrain, and from E11 within the cortex and terminates by E17 (Angevine & Sidman, 1961; Nornes & Carry, 1978). Early in neurogenesis neuroepithelial stem cells divide symmetrically to produce two stem cells, increasing the pool of progenitor cells (Jin et al., 2016). Embryonic neurogenesis begins with the transformation of neuroepithelial cells located in the VZ and subventricular zone into radial glial cells (Götz & Huttner, 2005; Huttner & Brand, 1997). Radial glial cells are fate-restricted neural stem cells that replace the neuroepithelial stem cell population (Anthony et al., 2004). Radial glial cells are bipolar and extend from the apical surface to the basal surface. Radial glial cells can divide symmetrically to self-renew or divide asymmetrically to produce progenitor cells or radial glial cells (Fietz & Huttner, 2011). Collectively, radial glial cells and neural progenitor cells are referred to as neural precursor cells (NPCs).

Neurons arise from progenitor cells either through asymmetric division of radial glial cells or through symmetric division of progenitor cells (Figure 1.1).

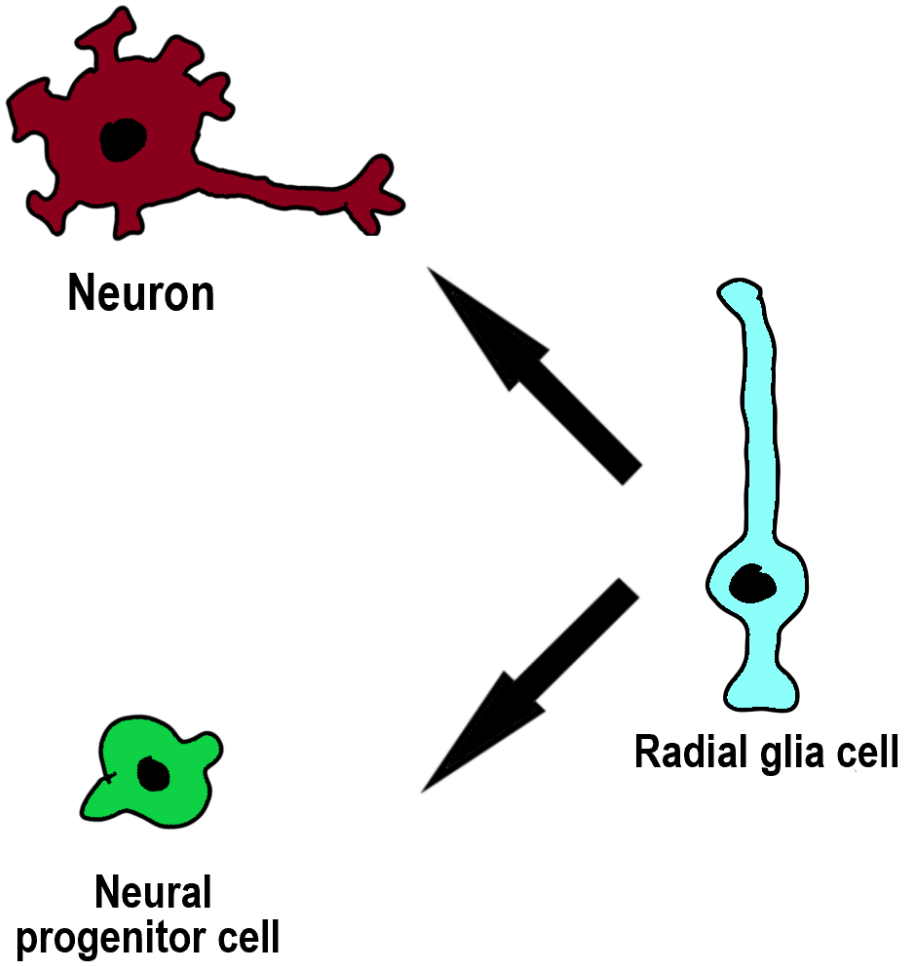

Figure 1.1: Neural precursor cells of the developing cerebral cortex.

The neural precursor cells of the developing cortex include the radial glial cells and the neural progenitor cells. These cells give rise to progenitor cells or can differentiate to become neurons (adapted with permission from Molnár et al., 2011).

During the early stages of cortical development, asymmetric division of radial glial cells gives rise to the majority of newly differentiated neurons (Miyata et al., 2001; Noctor et al., 2001). By mid-neurogenesis, neurons primarily arise from the symmetric division of progenitor cells (Haubensak et al., 2004; Noctor et al., 2004). Newly differentiated neurons use radial glial fibers to migrate to the cortical plate (Rakic, 1988). The cortex is formed in an "inside out" fashion, in which the earliest-born neurons make up the deepest layer of the cortex (Angevine & Sidman, 1961).

1.12 The role of mitochondria in developmental neurogenesis

Mitochondria are double membrane organelles, traditionally known for being the energy source of the cell through adenosine triphosphate (ATP) production. Though past research has primarily examined developmental signaling, transcriptional and epigenetic pathways during neurodevelopment, recent studies have demonstrated an essential role of mitochondria in stem cell regulation and fate decisions (Hu et al., 2016; Khacho et al., 2016). Mitochondrial function and morphology changes occur at the onset of differentiation and are a necessary process during neurogenesis (Homem et al., 2014; Stoll et al., 2015).

Differentiation of NSCs to postmitotic neurons is marked by a metabolic switch from glycolysis to oxidative phosphorylation (OXPHOS) (Beckervordersandforth et al., 2017; Khacho et al., 2016, 2017; Llorens-Bobadilla et al., 2015). NSCs rely on glycolysis for their metabolism (Agathocleous et al., 2012; Homem et al., 2014; Khacho et al., 2016; Zheng et al., 2016), while mature neurons depend on OXPHOS in order to meet the high-energy requirements necessary for cellular function, presynaptic vesicle recycling and the

generation of action potentials (Hall et al., 2012; Alle & Geiger, 2009). The metabolic switch from glycolysis to OXPHOS occurs progressively during neurogenesis, accompanied by alterations in metabolic enzyme expression (Figure 1.2) (Beckervordersandforth et al., 2017; Khacho et al., 2016, 2017; Llorens-Bobadilla et al., 2015).

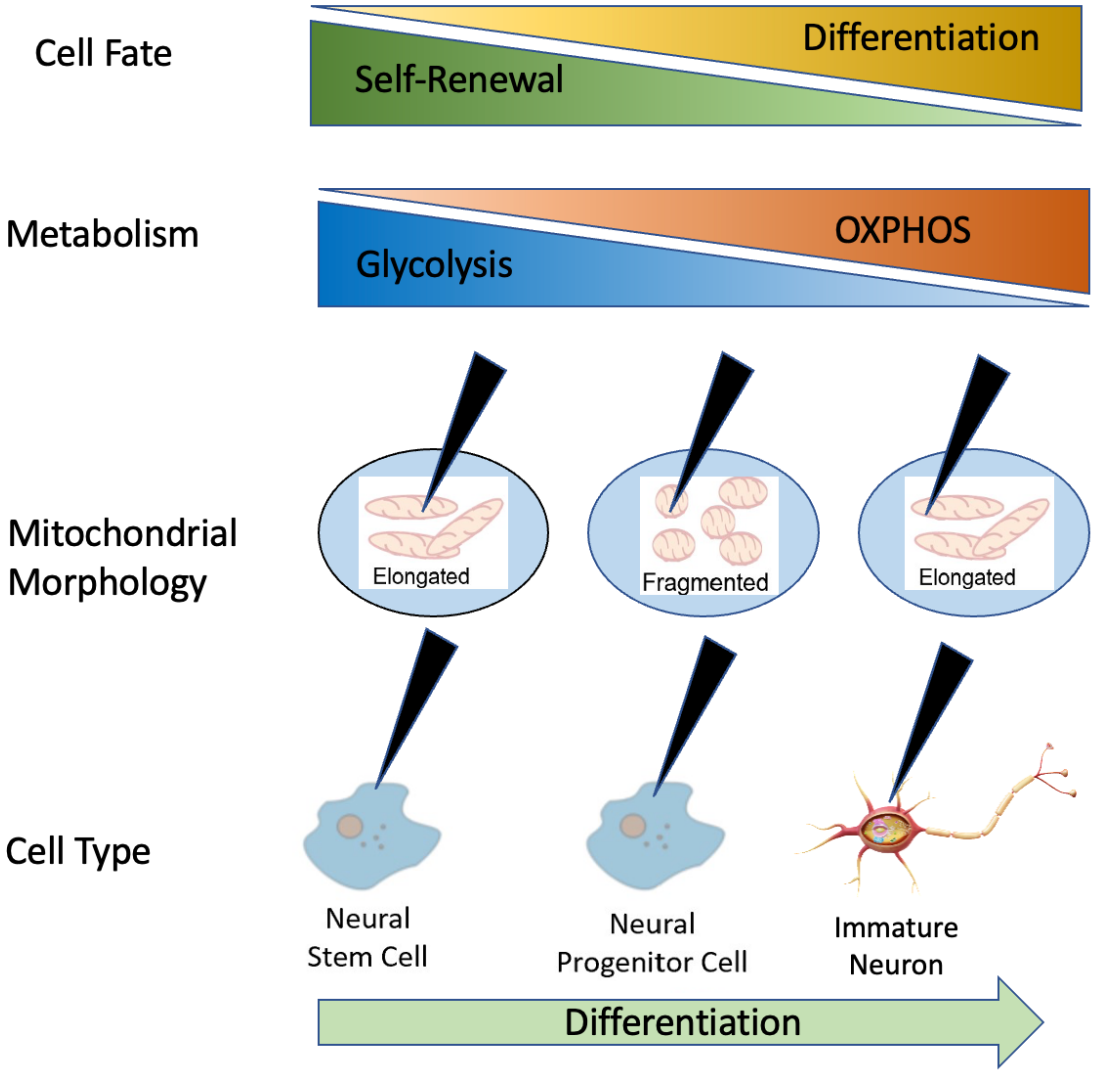

Figure 1.2: Mitochondria undergo morphological changes coincident with a metabolic switch from glycolysis to OXPHOS in cells during developmental neurogenesis

Mitochondria undergo alterations in structure coincident with a metabolic switch in cells during developmental neurogenesis. Neurogenesis is marked by a metabolic switch from glycolysis to OXPHOS. Mitochondria become fragmented upon differentiation of neural progenitor cells and return to an elongated state in neurons. ROS production increases in differentiating neural progenitor cells (adapted with permission from Khacho et al., 2019).

Studies have demonstrated that the metabolic switch from glycolysis to OXPHOS is not only a required transition for neurons to meet their increased energy requirements, but also is a regulatory step in neuron differentiation (Khacho et al., 2019).

Mitochondria undergo morphological changes during neurogenesis. In NSCs, mitochondria are elongated and remain elongated during the self-renewal phase (Khacho et al., 2016). Upon differentiation to neural progenitor cells, mitochondria become fragmented but return to an elongated morphology in postmitotic neurons (Figure 1.2). Mitochondrial morphological changes during differentiation are mediated by mitochondrial fission and fusion dynamics. In mouse and human NSCs, inhibiting fission results in daughter cells remaining in the self-renewal cycle, while promoting fission results in differentiation of daughter cells (Iwata et al., 2020). Morphological changes that occur within the postmitotic period of fate plasticity alters NSC fate, demonstrating the importance of mitochondrial remodeling during this phase of neurogenesis (Iwata et al., 2020).

Mitochondrial function and morphology mediate NPCs differentiation through modifying reactive oxygen species (ROS) signaling during neurogenesis (Khacho et al., 2016). In elongated mitochondria, NSCs maintain a low level of ROS production. The transition to a fragmented mitochondrial morphology in neural progenitor cells results in an increase in ROS, which promotes differentiation (Khacho et al., 2016). The increase in ROS inhibits the expression of the NSC self-renewal gene, *Botch,* and thereby promotes differentiation (Khacho et al., 2016). Increases in ROS results in the activation of differentiation gene expression, such as Insulin gene enhancer protein (*Isl1*), LIM homeobox protein 5 (*Lhx5*), NK2 Homeobox 1 (*Nkx2.1*) and SIM BHLH transcription factor 1 (*Sim1*) through a nuclear factor erythroid 2-related factor 2 (*NRF2*) dependent

retrograde pathway (Khacho et al., 2016). Therefore, mitochondrial metabolic activity and morphological changes mediate alterations in ROS levels, that in turn suppresses self-renewal of the NSC population and favor differentiation (Khacho et al., 2016).

Functional mitochondrial are essential during neurogenesis. Defects in mitochondrial function impacts NSC self-renewal, neuronal commitment and differentiation (Khacho et al., 2017). Similarly, mitochondrial dysfunction contributes to a decline in hippocampal neurogenesis associated with aging (Beckervordersandforth et al., 2017). Defects in mitochondrial function and morphology during neurodevelopment are associated with various neurodevelopmental disorders, such optic atrophy, tuberous sclerosis complex and schizophrenia (Hjelm et al., 2015; Rajasekaran et al., 2015). Therefore, further understanding of the cellular pathways and mechanisms that mediate mitochondrial function and morphology during neurogenesis is necessary.

1.2 Apoptosis

The term apoptosis was first used by Kerr, Wyllie and Currie to describe a distinct form of cell death (Kerr et al., 1972). Apoptosis or programmed cell death is an evolutionarily conserved cell death pathway. Cells undergo a process of controlled death without spillage of their contents into the surrounding environment (Kerr et al., 1972). Cell morphological characteristics of apoptosis include condensation of cellular contents, nuclear membrane breakdown, chromatin condensation, DNA fragmentation and breakdown of the cell into membrane-bound vesicles termed “apoptotic bodies” (Kerr, Wylie & Currie., 1972). Apoptosis occurs rapidly, with the entire process occurring within several hours (Bursch et al., 1990). Apoptosis can be initiated by either internal or external stimuli resulting in activation of either the intrinsic or extrinsic pathway. The extrinsic pathway is initiated through signaling between immune cells and a damaged cell, while the intrinsic pathway is initiated through signaling from a variety of stimuli acting on various targets within a cell (D’Arcy, 2019). Ultimately, apoptosis results in clearance of cells with minimal damage to surrounding tissue (D’Arcy, 2019).

1.2.1 Developmental Apoptosis

Apoptosis is vital for shaping the developing nervous system during embryogenesis (Dekker et al., 2013). Prior to the onset of neurogenesis, NSCs proliferation increases, resulting in a large expansion of their numbers (Haubensak et al., 2004; Gotz & Huttner, 2005). This period of increased proliferation is followed by a wave of apoptosis (Hamburger et al., 1981; Oppenheim, 1991). Apoptosis occurs in various regions of the CNS and peripheral nervous system (PNS), in neural precursor cells, differentiated postmitotic neurons and glial cells (Burek & Oppenheim, 1996; Kristiansen & Ham, 2014; Oppenheim, 1991). Furthermore, apoptosis occurs during various stages of nervous system development, including neurulation and synaptogenesis (Clarke et al., 1998; Depaepe et al., 2005; Finlay et al., 1989; Haydar et al., 1999; Kuan et al., 2000). Apoptosis during development of the nervous system ensures the regulation of the progenitor population, removes damaged cells, optimizes synaptic connections and pattern formation (Clarke et al., 1998; Depaepe et al., 2005; Finlay et al., 1989). However, once neurons become mature and integrate into functional circuits, their capacity to undergo cell death via apoptosis is greatly restricted. This restriction of apoptosis in neuronal maturation ensures their long-term survival (Hollville et al., 2019). Ultimately, developmental apoptosis ensures the establishment and patterning of the nervous system.

1.2.2 Intrinsic Apoptotic Pathway

The intrinsic apoptotic pathway is referred to as the mitochondrial pathway of apoptosis (Figure 1.3). Initiation of intrinsic apoptosis can occur in response to various cellular stresses, absence of cytokines, deprivation of trophic factors, DNA damage or endoplasmic reticulum stress (Hollville et al., 2019). Such initiators lead to mitochondrial outer membrane permeabilization (MOMP). MOMP is a critical process in which cells commit to undergoing apoptotic cell death, resulting in the release of cytochrome c from the mitochondria. Cytochrome c is located in the mitochondrial intermembrane space, which upon release binds to the apoptotic protease activating factor 1 (Apaf-1) during apoptosis (Liu et al., 1996). Apaf-1 contains a caspase recruitment domain (CARD), which in non-apoptotic cells is folded in such a way that its CARD domain is blocked. Apaf-1 forms a multimeric complex with cytochrome c and is referred to as the apoptosome, exposing its CARD domain, resulting in the recruitment of procaspase-9 (Li et al., 1997; Zou et al., 1997). The cleavage of pro-caspase 9 results in the activation of caspase-9, which subsequently activates downstream caspases such as caspase-3, caspase-6 and caspase-7 (Li et al., 1997; Zou et al., 1997). In its active form, caspase-3 induces apoptosis. Though intrinsic apoptosis involves complex interactions of various receptors, enzymes and proteins, it is primarily regulated by the Bcl-2 family of proteins.

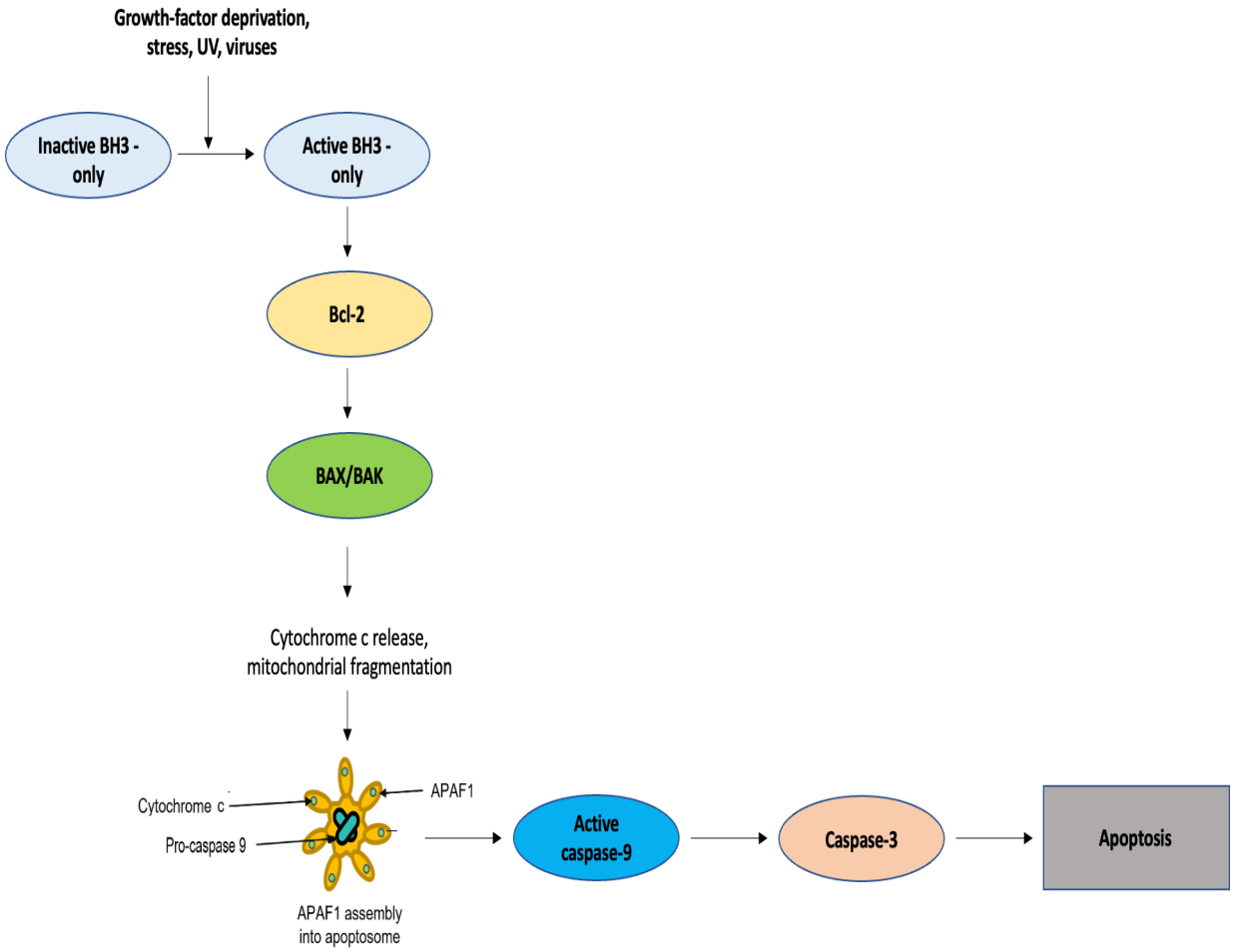

Figure 1.3: The intrinsic apoptotic pathway.

Intrinsic apoptosis is induced through various stimuli such as growth-factor depletion. Activation of pro-apoptotic Bcl-2 family members results in permeabilization of the outer mitochondrial membrane and subsequent cytochrome c release. The assembly of the apoptosome and activation of caspase-3 results in apoptosis (adapted with permission from Youle & Strasser, 2008).

1.3 Bcl-2 family

The Bcl-2 family of proteins consists of more than 20 proteins that regulate the intrinsic apoptosis pathway through controlling MOMP and the subsequent release of cytochrome c (Figure 1.4). The *Bcl-2* gene was first identified in patients with follicular lymphoma (Tsujimoto et al., 1985) and promoted malignant cell survival by preventing apoptosis (Ashkenazi et al., 2017; McDonnell et al., 1989; Vaux et al., 1988). All members of the Bcl-2 family contain at least one Bcl-2 homology (BH) domain, which contribute to all Bcl-2 proteins ability to regulate apoptosis (Kale *et al.,* 2017). Members of the Bcl-2 family are classified into three groups related to their structural and functional properties: pro-apoptotic proteins, BH3-only proteins, and anti-apoptotic proteins.

Pro-apoptotic proteins include Bcl-2 associated x (Bax) and Bcl-2 antagonist/killer-1 (Bak). Both Bax and Bak share BH1, BH2, BH3, and BH4 domains (Figure 1.4) (Henshall & Engel, 2013). Bax and Bak are localized to the outer mitochondrial membrane (OM) in their inactive conformations (Heath-Engel & Shore, 2006). Furthermore, the function of Bax and Bak are inhibited when bound to anti-apoptotic Bcl-2 protein members (Hardwick & Soane, 2013; Oltval, Milliman, & Korsmeyer., 1993). Bax and Bak promote MOMP through their oligomerization and subsequent pore formation in their active conformation. This increase in MOMP results in the subsequent release of cytochrome c from the mitochondrial inner membrane space into the cytosol (Cosulich et al., 1997; Kim et al., 1997; Jurgensmeier et al., 1998; Rosse et al., 1998; Kluck et al., 1999).

BH3 only proteins included Bcl-2 interacting mediator of cell death (BIM), p53 upregulated modulator of apoptosis (PUMA), BH3 interacting death domain agonist (BID), Bcl-2 interacting killer (BIK), Bcl-2 associated death promoter (BAD), Bcl-2 modifying

factor (BMF), Harakiri Bcl-2 interacting protein (Hrk) and NOXA. All members contain only the BH3 domain, though lack overall amino acid sequence similarity to other Bcl-2 family members or to each other (Figure 1.4) (Hardwick & Soane, 2013; Huang & Strasser., 2000; Shamas-Din et al., 2011). BH3-only proteins initiate apoptosis through two strategies; by directly binding and stimulating pro-apoptotic proteins Bax and Bak or indirectly by binding to specific anti-apoptotic proteins (Billen et al., 2008; Deng et al., 2007; Petros et al., 2000). Unlike the pro-apoptotic and anti-apoptotic proteins, BH3-only proteins are transcriptionally or post-translationally active in response to apoptotic stress signaling (Engel et al., 2011)

Anti-apoptotic proteins include Bcl-2, Bcl-2-related gene long isoform (Bcl-xL), myeloid cell leukemia 1 (Mcl-1) and Bcl-2 related protein A1 (A1). The anti-apoptotic proteins contain BH1, BH2, BH3, and BH4 domains (Figure 1.4). All members contain a C-terminal transmembrane domain that localizes them to intracellular membranes such as the mitochondrial outer membrane (Brunelle and Letai, 2009; Chipuk et al., 2006; Cory and Adams, 2002; Tait and Green, 2010). Anti-apoptotic proteins inhibit the actions of pro-apoptotic proteins through binding to their BH3 motifs (Billen et al., 2008; Cheng et al., 2001).

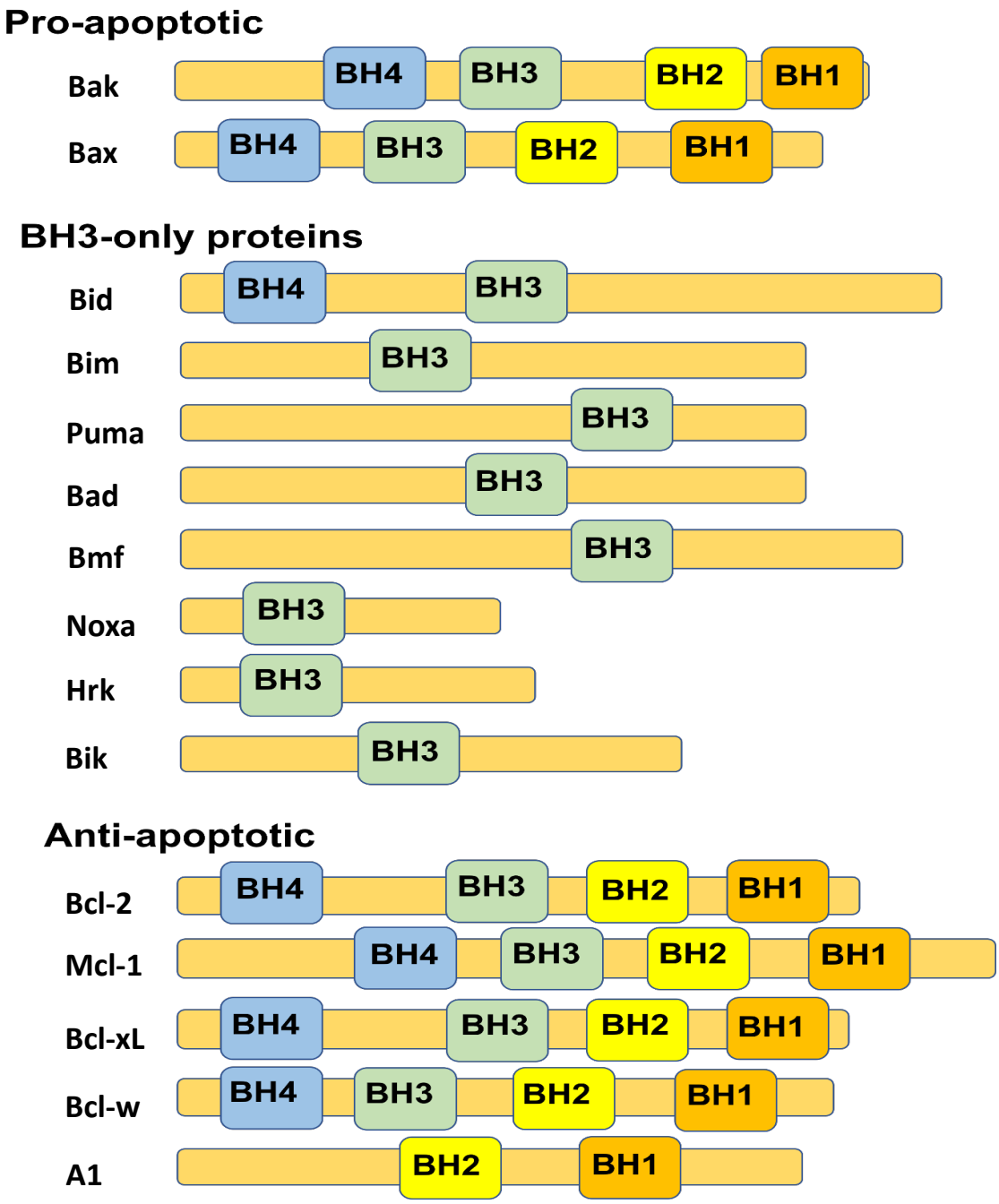

Figure 1.4: The Bcl-2 family of proteins

The Bcl-2 family of proteins regulates apoptosis through mediating MOMP. The Bcl-2 family consists of three major groups: the pro-apoptotic proteins, the anti-apoptotic proteins, and the BH-3 only proteins (adapted with permission from Youle & Strasser, 2008).

1.3.1 The role of Bcl-2 family members in developmental neurogenesis

Gene knock-out studies have been critical in identifying members of the Bcl-2 family that are necessary for nervous system development. Knock-out of the individual BH3-only proteins, the pro-apoptotic protein BAK as well as the anti-apoptotic members A1 or Bcl-w have not demonstrated an essential role in nervous system development (Bouillet et al., 1999; Michaelidis et al., 1996; Leonard et al., 2001; Lindsten et al., 2000; Print et al., 1998; Ranger et al., 2003; Ross et al., 1998; Schenk et al., 2017; Shibue et al., 2003; Tuzlack et al., 2017; Vilunger et al., 2003). In contrast, Bcl-2, Bcl-xl, Mcl-1, and Bax play distinct roles during nervous system development.

Bcl-2 is widely expressed during early neurulation (E4.5-8) though expression declines in the CNS after neural tube formation (E10-11) but persists in the adult PNS (Abe-Dohmae et al., 1993; Merry et al., 1994). Reduction of *Bcl-2* expression continues in the postnatal brain; however, higher levels of expression are observed in the PNS including sensory and sympathetic neurons (Abe-Dohmae et al., 1993; Merry et al., 1994). *Bcl-2* deficient embryos do not exhibit phenotypic alterations during nervous system development, though deletion of *Bcl-2* postnatally results in the loss of motor neurons of the facial nucleus, sensory neurons of the dorsal root ganglia, and sympathetic neurons of the superior cervical ganglia (Michaelidis et al., 1996). These studies ultimately demonstrate an essential role of Bcl-2 in neuronal survival in the postnatal nervous system.

Bcl-xL is essential for embryonic development, as germline deletion of *Bcl2l2,* the gene encoding Bcl-xL, results in embryonic death by E13.5 with substantial apoptosis in the nervous system and hematopoietic systems (Motoyama et al., 1995). Bcl-xL is expressed at low levels during nervous system development but increases expression at the onset of

neurogenesis (Fogarty et al., 2016). Bcl-xL is essential for the survival of the nervous system during developmental neurogenesis. Conditional deletion of Bcl-xL in the nervous system using the cre/lox system with the Nestin promoter as the driver of Cre recombinase expression results in apoptosis starting at E11 in the ventrolateral spinal cord and peaking at E13 throughout the nervous system (Fogarty et al., 2016). Furthermore, apoptosis occurred in cells that had exited the cell cycle within the last 24 hours (24H) according to the spatial and temporal sequence of neuronal differentiation (Fogarty et al., 2019). Conditional deletion of Bcl-xL using the Emx1 promoter to drive Cre expression resulted in apoptosis of post-mitotic neurons in the upper layers of the cortex from post-natal day 1 to 30 (Nakamura et al., 2016). Bcl-xL is required for the survival of select neuron populations including: catecholaminergic neurons, upper layer cortical neurons, CA1-CA3 hippocampal neurons, spinal cord interneurons and motor neurons (Nakamura et al., 2016; Fogarty et al., 2016; Savitt et al., 2005). These studies demonstrate an essential role of Bcl-xL in the survival of post-mitotic neurons.

The pro-apoptotic protein Bax is expressed during developmental neurogenesis, with increasing protein expression in differentiating neurons (Krajewska et al., 2002). However, Bax decreases in expression postnatally (Polster et al., 2003). Bax promotes cell death in the developing CNS (Hardwick & Soane, 2013; Sun et al., 2004). Germline deletion of Bax (Bax Null) rescues neurons from developmental death, resulting in increases in neuronal populations of the superior cervical ganglia and facial nuclei (Deckwerth et al., 1996). Recent studies have demonstrated that Bax is a common pro-apoptotic target for Mcl-1 and Bcl-xL during developmental neurogenesis (Flemmer et al., 2021; Fogarty et al., 2019;

Shindler et al., 1997). Such studies demonstrate that Bax exerts its pro-apoptotic functions during developmental neurogenesis.

1.3.2 Bcl-2 family involvement in non-apoptotic functions

Recently, Bcl-2 family members have been identified in roles distinct from apoptosis. Bax is located on the outer mitochondrial membrane and interacts with known fission protein dynamin related protein-1 (Drp-1) and known fusion proteins mitofusion-1 (MFN1) and MFN2 (Kabarski et al., 2002). The soluble form of Bax stimulates fusion through a MFN2-dependent manner (Hoppins et al., 2011). Bax plays a role in mitochondrial fission, which is required for mitochondrial fragmentation observed in apoptotic cells (Maes et al., 2019). Bax colocalizes with Drp-1 during apoptosis, thereby affecting mitochondrial fission (Karbowski et al., 2002). Furthermore, the interaction of Drp-1 and Bax results in mitochondrial permeability transition pore opening after hypoxia in cardiomyocytes, resulting in mitochondrial dysfunction and cell death (Duan et al., 2021). A study by Joshi et al. (2020) demonstrated that deletion of Bax and Bak resulted in abnormal mitochondrial cristae structure and loss of mitochondrial mass, but no defects in ATP production, in both human-induced pluripotent stem cells and NPCs. It is evident that Bax is involved in mitochondrial fission/fusion dynamics in tandem with its pro-apoptotic functions; however, it is currently unknown whether Bax exerts such functions during developmental neurogenesis.

Bcl-xL maintains mitochondrial membrane potential and membrane integrity by inhibiting mitochondrial membrane hyperpolarization and swelling in cells exposed to

apoptotic and necrotic stimuli (Vander Heiden et al., 1997). Bcl-xL interacts with voltage-dependent anion channels to promote calcium (Ca^{2+}) uptake (Huang et al., 2013). Studies in neurons have shown that Bcl-xL is located in the inner mitochondrial membrane (IMM), in addition to OM localization (Alavian et al., 2011; Chen et al., 2011). At the IMM, Bcl-xL increases ATP levels, oxygen consumption and influences the activity of F_1F_0 ATP synthase. Bcl-xL maintains mitochondrial membrane potential by inhibiting an ion leak pathway within the F_1F_0 ATP synthase (Alavian et al., 2011; Chen et al., 2011). Bcl-xL inhibits fission induced by Bax (Bleicken et al., 2016). To date, no analysis of mitochondria morphology or assessment of cellular respiration has been conducted in response to the loss of Bcl-xL during neurogenesis. Therefore, whether Bcl-xL's role in the maintenance of mitochondrial activity and integrity impacts its pro-survival function during developmental neurogenesis remains unknown.

1.4 Myeloid cell leukemia 1 (Mcl-1)

Mcl-1 is an anti-apoptotic member of the Bcl-2 family. Unlike other members of the Bcl-2 family, the expression of Mcl-1 is tightly regulated, and the protein has a short half-life of roughly two hours (Warr et al., 2005; Zhong et al., 2005). Furthermore, Mcl-1 is predominantly localized to mitochondria (Yang et al., 1995). Mcl-1 exerts its anti-apoptotic function by inhibiting the actions of the pro-apoptotic proteins. Specifically, Mcl-1 sequesters Bak and blocks the translocation of Bax to mitochondria (Cheng et al., 2007; Willis et al., 2005). Mcl-1 can inhibit apoptosis through interactions with BH3-only protein members such as NOXA (Mei et al., 2007).

1.4.1 The role of Mcl-1 in developmental neurogenesis

Mcl-1 is essential for NPCs survival early in neurogenesis after neural tube formation, as NPCs exit the cell cycle to differentiate (Arbour et al., 2008; Fogarty et al., 2019). Germline knock-outs of Mcl-1 are peri-implantation lethal at E3.5 (Rinkenberger et al., 2000). Conditional knockout of Mcl-1 (MKO) in the nervous system using the Cre/lox system results in widespread NPCs apoptosis beginning at E9 in the brainstem and spinal cord (Flemmer et al., 2021) and at E10 in the developing forebrain NPCs population (Fogarty et al., 2019). Embryonic lethality occurred by E16, demonstrating that Mcl-1 is a crucial survival factor for NPCs (Arbour et al., 2008). The dependency on Mcl-1 for survival from an apoptotic fate changes as neurogenesis progresses, as post-mitotic neurons become more resistant to apoptosis (Annis et al., 2016; Germain et al., 2011; Kole et al., 2013; Veleta et al., 2020). These studies demonstrate the dynamic role of Mcl-1 in promoting the survival of NPCs during neurogenesis.

1.4.2 Mcl-1's non-apoptotic function

Mcl-1 has roles distinct from apoptosis, such as differentiation. Mcl-1 was first identified as a gene upregulated during lymphoid cell differentiation (Kozopas et al., 1993). Harley et al. (2010) demonstrated that Mcl-1 expression varies throughout the cell cycle, peaking in M-phase as cells begin to differentiate. Mcl-1 overexpression in NPCs causes premature NPCs differentiation (Hasan et al., 2013).

Mcl-1 has a role in mitochondrial activity and integrity. Post-translational processing of Mcl-1 occurs in the mitochondria resulting in two isoforms that have distinct locations within the mitochondria. The Mcl-1^{OM} isoform, first identified in cardiomyocytes is located on the OM where it antagonizes the activity of Bax and Bak to prevent apoptosis

(Perciavalle et al., 2012). Mcl-1 interacts with fission/fusion proteins Drp-1 and Opa1 mitochondrial dynamin like GTPase (Opa-1) and inhibiting or silencing Mcl-1 results in alterations to the mitochondrial networks as mitochondria become more elongated (Rasmussen et al., 2018). This may in part be a function of Mcl-1^{OM} due to the location of fission/ fusion proteins on the OM, but remains to be determined. The Mcl-1^{matrix} isoform is located within the mitochondrial matrix and regulates mitochondrial bioenergetics through promoting membrane potential, ATP production, mitochondrial fusion, normal IMM structure and assembly of the F_1F_0ATP synthase oligomers (Perciavalle et al., 2012). Furthermore, Mcl-1^{matrix} enhances respiratory function by modulating mitochondrial oxygen consumption and Ca^{2+} retention in neurons while inhibiting mitochondrial permeability pore opening during stress conditions (Anilkumar et al., 2020). Similar to neurons, loss of Mcl-1 in cardiomyocytes results in abnormal mitochondrial cristae ultrastructure and defects in mitochondrial respiration (Wang et al., 2014). Though the function of Mcl-1 in mitochondrial bioenergetics, morphology, and cellular respiration has been described in post mitotic neurons during stress conditions, how Mcl-1 affects mitochondrial bioenergetics and morphology in NPCs during neurogenesis has yet to be examined.

1.5 Research Rationale

Mcl-1 is essential for nervous system development. Research from our laboratory has demonstrated Mcl-1 promotes NPCs survival by inhibiting the pro-apoptotic activity of Bax (Flemmer et al., 2021; Fogarty et al., 2019). This function is consistent with its location on the OM. As mitochondria play an integral role in neurogenesis, the role of Mcl-1 during this period has come into question. Mcl-1 has distinct functions from its anti-apoptotic role, and is involved in regulating mitochondrial activity and integrity. No morphological or functional analysis of mitochondria in response to loss of Mcl-1 has been conducted during the period of neurogenesis to date. Therefore, it remains elusive whether Mcl-1 mediates mitochondria activity and morphological dynamics during developmental neurogenesis.

This leads to my **hypothesis** that Mcl-1 functions to promote the transition from NPCs to immature neuron through its roles in mitochondrial dynamics during developmental neurogenesis.

To address this hypothesis, I have the following specific aims:

Aim 1: Does Mcl-1 impact cell cycle exit at the onset of neurogenesis, and is the observed phenotype rescued through co-deletion of Mcl-1 and Bax.

Aim 2: Examine the effect of loss of Mcl-1 on mitochondrial morphology, size and number through immunohistochemistry and electron microscopy during the timepoint when Mcl-1 is critical for survival during neurogenesis.

Chapter 2: Materials and Methods

2.1: Mice

Mice were kept on a 12 hour light/dark cycle and provided with food and water *ad libitum*. All experiments were approved by Memorial University's Institutional Animal Care Committee, adhering to the Guidelines of the Canadian Council on Animal Care.

Nestin Cre ($Cre^{+/-}$) transgenic mice were generated in the laboratory of Dr. R. Slack (Berube *et al.,* 2005) and *mcl-1* floxed mice were generated in the laboratory of Dr. S. Korsmeyer (Opferman *et al.,* 2005). *Bax* null (BaxN) mice were obtained from Jackson labs (002994, Bar Harbour, Maine, USA) (Knudson *et al.,* 1995). *Bax* floxed ($Bax^{f/f}$) mice were obtained from Jackson labs (004183, Bar Harbour, Maine, USA). All mice strains used in this study were maintained on a C57BL/6 background.

To generate conditional knockout (KO) of *mcl-1* (MKO), Cre+/- transgenic mice were bred with *mcl-1* floxed mice (Arbour *et al.,* 2008). To generate Mcl-1 CKO:Bax CKO double conditional knockout mice (MKO: BaxKO), *Bax* null/floxed mice were bred with Mcl-1 CKO mice (Fogarty *et al.,* 2019).

Breeding pairs were placed in the same cage until the formation of a vaginal plug was observed, up to a maximum of three days. Female mice were checked for the presence of a vaginal plug twice daily, once in the early morning and again in the early evening. E0.5 was designated upon the detection of a vaginal plug. Upon detection of a vaginal plug, male mice were removed from the cage and female mice were weighed. Female mice were weighed on a weekly basis to confirm pregnancy status.

BrdU (Millipore Sigma, B5002, Oakville, Ontario, Canada) was injected intraperitoneally (50 μg/g body weight) in pregnant mice at E10, 24 hours prior to sacrifice. EdU (Sigma, 900584, Oakville, Ontario, Canada) was injected intraperitoneally (50 μg/g body weight) at E11, 2 hours prior to sacrifice.

2.2: Genotyping

Tissue samples were collected from embryonic mouse tails and/or limbs at the time of dissection for genotyping. Tail clippings were taken from mice at weaning for genotyping. DNA was extracted using the REDExtract-N-Amp tissue PCR kit (Sigma, XNAT2, Oakville, Ontario, Canada). Briefly, 50 μL of extraction solution and 12 μL of tissue prep were added to each tissue sample and then the samples were vortexed. The samples were then incubated in a water bath at 55°C overnight or until the tissue samples were completely digested. The samples were then heated at 100°C for 3 min followed by the addition of 50 μL of neutralizing solution to each sample to stop the digestion reaction. Polymerase chain reaction (PCR) was then performed. The reaction components and conditions for each PCR performed are listed in Tables 2.1 and 2.2. PCR samples and loading dye (30% Glycerol, 1mM EDTA, 0.06% BPB) were loaded and run in a 2% agarose gel (UltraPure Agarose – Invitrogen 16500500, Burlington, Ontario, Canada) containing 3 μL of ethidium bromide (15585-011, Invitrogen) at 120 volts (V). The samples were run for approximately 45 min to detect the presence of the *cre*, *Bax null* and $Bax^{f/f}$ alleles. The samples were run for approximately 90 min to ensure separation of the *mcl-1* floxed allele, detected by the presence of a 400 base pair (bp) band, and 360 bp wildtype allele. Gel bands were visualized under ultraviolet light. The presence of *cre* was determined by the presence of a single band of 700 bp.

mcl-1 wildtype alleles were determined by the presence of a 360bp band while *mcl-1* floxed alleles were determined by the presence of a 400 bp band. The *bax null* allele was determined by the presence of a 507 bp band while the *bax* wild type allele was determined through the presence of a 304 bp band. The $bax^{f/f}$ allele was determined by the presence of a 244 bp band.

Table 2.1: The reaction components for the cre, *mcl-1, bax null and bax$^{f/f/}$* PCR used for genotyping

Reagent	**Cre PCR Volume (µL/tube)**	***mcl-1* PCR Volume (µL/tube)**	***Bax null* PCR Volume (µL/tube)**	***Bax f/f* PCR Volume (µL/tube)**	***SRY PCR* Volume (µL/tube)**
5X OneTaq Reaction buffer	10	10	10	N/A	10
RedExtract-N-AMP buffer	N/A	N/A	N/A	10	N/A
FOR Primers (2.5µM)	4.0	5.0	5.0	3.2	5.0
REV Primers (2.5µM)	4.0	5.0	10.0	3.2	5.0
Neo/pgk Primer (2.5µM)	N/A	N/A	Bax2 – 5.0	N/A	N/A
1.25mM dNTPs	8	8	8	N/A	8
OneTaq Polymerase	0.25	0.25	0.25	N/A	0.25
Water	21.75	17.75	7.75	1.6	17.75
DNA sample	2.0	4.0	4.0	2.0	4.0

Cre-3b FOR	5’- TGACCAGAGTCATCCTTAGCG – 3’
Cre-5b REV	5’- AATGCTTCTGTCCGTTTGCC – 3’
6 *mcl-1* FOR	5’- GCAGTACAGGTTCAAGCCGATG-3’
7 *mcl-1* REV	5’- CTGAGAGTTGTACCGGACAA – 3’
Bax3.1 FOR	5′-TGATCAGAACCATCATG-3′
Bax1 Neo/pgk	5′-GTTGACCAGAGTGGCGTAGG-3′
Bax2 REV	5′-CCGCTTCCATTGCTCAGCGG-3′
Baxf FOR primer	5’-GAATGCCAAAAGCAAACAGACC-3’ 5’-ACTAGGCCCGGTCCAAGAAC-3’
Baxf REV primer	5’-GTC AAG CGC CCC ATG AAT GG-3’ 5’-TAG TTT GGG TAT TTC TCT CT-3’
SRY BA primer	
SRY FA primer	

Table 2.2: The reaction conditions for the *cre, mcl-1, bax null and bax$^{f/f/}$* PCR used for genotyping

Steps	***Cre* PCR**		***Mcl-1* PCR**		***Bax null* PCR**		***Bax*$^{f/f}$ PCR**		***SRY* PCR**	
1	94°C for 5 min		94°C for 5 min		94°C for 5 min		94°C for 3 min		94°C for 3 min	
2	94°C for 1 min	Steps 2-4	94°C for 1 min	Steps 2-4	94°C for 1 min	Steps 2-4	94°C for 30 sec	Steps 2-4	94°C for 30 sec	Steps 2-4
3	56°C for 1 min	X30 cycles	56°C for 1 min	X30 cycles	55°C for 1 min	X30 cycles	68°C for 1 min	X35 cycles	55°C for 1 min	X30 cycles
4	72°C for 1.5 min		72°C for 1 min		72°C for 1 min		72°C for 1 min		72°C for 1 min	
5	72°C for 5 min		72°C for 1 min		72°C for 3 min		72°C for 2 min		72°C for 10 min	
6	10°C forever		10°C forever		10°C forever		10°C forever		10°C forever	

2.3: Embryonic Tissue Collection and Preparation

Tissue collection for embryonic mice occurred at E11. Pregnant mice were euthanized with an intraperitoneal injection of Euthanyl (300 mg/mL sodium pentobarbital-Vètoquinol, IEUS001, Lavaltrie, Quebec, Canada) followed by cervical dislocation. The abdomen was wiped with 70% ethanol (EtOH) and a midline cut through the skin followed by a cut through the peritoneum was performed. The uterus was removed and the embryos were collected and placed in individual dishes containing 1X Hanks' Balanced Salt Solution (1X HBSS) (Fisher, 14065-056, Ottawa, Ontario, Canada), pH 7.4. Embryos were removed from the embryonic sac and surrounding membrane. The tail limb and/or body of the embryo was collected for genotyping. The brains were then dissected from the embryos. This was accomplished by first separating the embryonic head from the body through separation between the second and third branchial arch. The embryonic brains were placed in dishes containing 1X HBSS.

Following dissection, the embryonic brains were fixed in 4% paraformaldehyde (PFA) in 1X phosphate buffered saline (137 mM NaCl, 2.7 mM KCL, 10 mM Na_2HPO_4 , 1.8 mM KH_2PO_4 (PBS)), pH 7.4 overnight. After the fixation period, embryos were cryoprotected through a successive series of sucrose solutions w/v in 1X PBS (12%, 22% and 30%). Cryoprotection was considered successful upon the equilibrium of the brain tissue with the solution. Following cryoprotection, the brains were mounted in Tissue-Tek OCT Compound (Somagen Diagnostics, 4583, Sakura Finetek, California, United States) embedding medium in a cryomold and positioned in the orientation required for sectioning. Brains were frozen in isopentane cooled on dry ice for approximately 3 min. After freezing, brains were stored at -80°C.

Brains were sectioned in a cryostat (Microm HM 520, Fisher Scientific, Ottawa, Ontario, Canada) in the coronal plane at a thickness of 14 µm at -23°C. Brain sections were collected in a series across six slides, such that sections on each slide represented sections 140 µm apart in the anterior-posterior axis through the brain. Sections were collected on Superfrost Plus slides (Fisher, 1255015, Ottawa, Ontario, Canada). After sectioning, the slides were stored at -80°C.

2.4: Immunohistochemistry

Slides were warmed at 37°C for 30 min prior to immunohistochemistry. During the warming period, a PAP pen (Dako, S2002, Denmark) was used to draw a hydrophobic barrier surrounding the tissue sections on each slide.

Pre-treatment was required for BrdU and Cut like homeobox 1 (Cux1+) following the warming period. For BrdU and Cux1+ immunohistochemistry, slides were washed in acetone for 3 min at room temperature to fix the tissue. For BrdU immunohistochemistry, slides were then placed in 2 N hydrochloric acid (HCL) for 30 min at 37°C as a denaturation step, followed by neutralization in 0.1 M sodium borate pH 8.0 for 10 min at room temperature.

All slides were then washed twice in 1X PBS for 5 min. Following the washes, the slides were incubated with the appropriate primary antibody diluted in 1X PBS at room temperature overnight in a humidity chamber, as outlined in Table 2.3.

After the incubation period, the slides underwent 3 washes in 1X PBS for 10 min each. The slides were then incubated in the dark in a humidity chamber at room temperature for 1 hour with the appropriate secondary antibody (Table 2.4). Following incubation, slides were

washed twice in 1X PBS for 10 min, then stained with the nuclear dye Hoechst (1:250 BisBenzimide H33258- Sigma, B1155, Oakville, Ontario, Canada) diluted in 1X PBS for 3 min. Next, slides underwent two subsequent washes in 1X PBS for 5 min each, and then were coverslipped using a solution of 1:3 glycerol: 1X PBS. Coverslips were sealed with nail polish. After drying at room temperature for several hours, the slides were stored at -20°C until microscopy.

Table 2.3: List of primary antibodies for immunohistochemistry

Primary Antibody	**Antibody Dilution**	**Marker**	**Source, Catalogue #, Location**
Active Caspase 3	1:400	Apoptotic cells	BD Biosciences, 559565, Mississauga, Ontario, Canada
BrdU	1:100	Proliferation	BD Biosciences, 347580, Mississauga, Ontario, Canada
Nestin	1:400	NPC	Millipore Sigma, MAB353, Oakville, Ontario, Canada
Tom20	1:100	Mitochondria	Santa Cruz, sc-11021, Dallas, Texas, U.S.A

Table 2.4: List of secondary antibodies for immunohistochemistry

Secondary Antibody	Antibody Dilution	Source, Catalogue #, Location
Alexa Fluor 488 Donkey (Anti Mouse)	1:200	Invitrogen, A21202, Burlington, Ontario, Canada
Alexa Fluor 488 Donkey (Anti Rabbit)	1:200	Invitrogen, A21206, Burlington, Ontario, Canada
Alexa Fluor 488 Donkey (Anti Goat)	1:200	Invitrogen, A11055, Burlington, Ontario, Canada
Alexa Fluor 594 Donkey (Anti Mouse)	1:200	Invitrogen, A21203, Burlington, Ontario, Canada
Alexa Fluor 594 Donkey (Anti Rabbit)	1:200	Invitrogen, A21207, Burlington, Ontario, Canada

2.5 Click-it EdU imaging

Slides were placed on a slide warmer at 37°C for 30 min prior to Click-iT® 5-ethynl-2'-deoxyuridine (EdU) treatment, and a hydrophobic barrier was drawn on the slide surrounding the tissue sections. After the warming period, the slides were placed in a 1:1 methanol : acetone solution at room temperature for 2 min as a fixation step. Next, slides were washed twice in 1X PBS for 10 min each followed by a wash in 1X PBS + 0.5% Triton X 100® (Sigma, 9002-93-1, Oakville, Ontario, Canada) for 10 min. The slides were then incubated in the dark in a humidity chamber at room temperature for 30 min with the Click-iT® EdU solution (Invitrogen, C10086, Burlington, Ontario, Canada). The reaction components of the Click-iT® EdU solution are listed in Table 2.5. Following incubation, the slides were washed in 1X PBS for 10 min and further stained with the nuclear dye Hoechst (1:250 BisBenzimide H33258- Sigma, B1155, Oakville, Ontario, Canada) diluted

in 1X PBS for 3 min. The slides were then washed twice in 1X PBS for 5 min each, and then were coverslipped using a solution of 1:3 glycerol: 1X PBS. Coverslips were sealed using nail polish, and the slides were stored at -20°C until microscopy.

Table 2.5: Click-it EdU reaction components

Reaction components	Volume (µL/sample)
1xClick-iT® reaction buffer	430
CuSO4 (Component E)	20
Alexa Fluor® azide	1.2
Reaction buffer additive	50
Total Volume	500

2.6: Cresyl Violet Staining

Slides selected for cresyl violet staining were warmed at 37°C for 30 min prior to the staining procedure. After warming, the selected slides were placed in 0.1% v/v filtered cresyl violet stain (0.5 g cresyl violet acetate, 250 mL distilled water, 750 µL glacial acetic acid, 126 µL NaOAc pH 5.2), pH 3.5 (Sigma, C1791-5G, Oakville, Ontario, Canada) for 30 min at room temperature. The selected slides were then washed in water, followed by v/v ethanol washes at increasing concentrations (50%, 70%, 90%, 95%, and three 100% washes), to dehydrate the tissue followed by an isopropanol wash and two toluene washes. All washes occurred for 30 seconds each. After the washes, the selected slides were cover-slipped after being mounted with Permount (Fisher, SP15-500, Ottawa, Ontario, Canada). Cresyl violet stained slides were stored at room temperature.

2.7 Microscopy and Cell Counting

Slides were viewed using a Zeiss AxioImager Z.1 microscope (Carl Zeiss Microscopy, Jenna, Germany). Fluorescence was produced using a Colibri LED light source (Carl Zeiss Microscopy, Jenna, Germany). All photomicrographs from selected slides were captured at 20X magnification using a Zeiss AxioCam MRm camera (Carl Zeiss Microscopy, Jenna, Germany) through the Zeiss AxioVision v4.8 software. All figures were created using Adobe Photoshop C2 (San Jose, CA, USA).

Cell counting was performed on four 14 µm thick coronal sections per embryo using ImageJ software (*http://rsbweb.nih.gov.qe2a-proxy.mun.ca/ij/*). The total number of cells, BrdU+ only cells, EDU+ only cells and double labelled BrdU+ and EdU+ cells were counted in one boxed area (200 µm X 100 µm) per section in the developing cerebral cortex and medial ganglionic eminence (100 µm X 200 µm) of E11 embryos. Apoptotic cells were quantified through condensed nuclei.

2.8 Super resolution imaging and measurements

To quantify mitochondria within NPCs in the medial ganglionic eminence, brain sections were co-immunostained with Tom20 antibodies to label mitochondria and Nestin antibodies to label NPCs. Immunostained sections (14 µm) were imaged through a EM CCD camera (Andor, iXon Ultra 897) and Olympus BX51 microscope, and a LED illumination source (Prior, Lumen 300) was used to excite the Alexa 594 fluorophore which labelled the Nestin antibody, and the Alexa 488 fluorophore which labelled the Tom20 antibody. A 60X oil

immersion objective (Olympus, 1.40NA) was used for imaging. The Andor Solis software program was used to take 100 images of each fluorophore.

Imaging of mitochondria was achieved using super-resolution radial fluctuations (SRRF). In brief, 100 images were loaded into FIJI (*https://imagej.net/software/fiji/*) , and super-resolution was constructed using the NanoJ-SRRF plugin. The pixel series of 100 images were cropped from 512 x 512 pixels to 128 x 128 pixels and auto local threshold was completed manually. The NPCs images, consisting of 100 images, were merged into 1 image through "Z project" to acquire an average intensity projection and converted to an 8 bit image. The NPCs and mitochondrial images were then merged using a previously described macro entitled "Colocalization", which was performed to quantify the number of mitochondria per NPCs (Wiemerslage & Lee, 2016). Mitochondrial number were measured per cell using a previously described macro entitled "Mitochondrial Morphology", which measured mitochondrial number, area (μm^2), perimeter (μm), circularity and elongation (Dagda et al., 2009). The threshold was adjusted to 20% of the maximum intensity, and the particle range was set to 5-500 pixels (Wiemerslage & Lee, 2016).

2.9 Electron Microscopy and measurements

The medial ganglionic eminence was dissected in 1X HBSS and incubated in 0.1 M sodium cacodylate buffer (Canemco-Marviac Inc, C0250-25g, Quebec, Canada). The tissue was stored in Karnovsky fixative (2% paraformaldehyde (Canemco-Marivac Inc., 30525-89-4, Quebec, Canada) and 2.5% Glutaraldehyde (Electron Microscopy Sciences, 16210, Hatfield, PA, USA) in 0.1M sodium cacodylate buffer) before tissue processing.

Processing and imaging of medial ganglionic eminence tissue was conducted by Memorial University's Medical Laboratories-Electron Microscopy Unit. The medial ganglionic eminence from E11 embryos was fixed in Karnovsky fixative for 20 min, and then transferred to 0.1 M sodium cacodylate buffer. The tissue then underwent a series of washes to dehydrate the tissue. First, the tissue was placed in 1% Osmium Tetroxide (Sigma, 75632, Oakville, Ontario, Canada) for 15 min, followed by a 0.1 M sodium cacodylate buffer for 5 min. The tissue then underwent v/v ethanol washes at increasing concentrations (two 70% washes for 10 min each, two 95% washes for 10 min each, and two 100% washes for 10 min each), and was then washed twice in absolute acetone for 10 min each. In order to infiltrate the tissue with epoxy resin (14.5 g Epoxy Embedding Medium (Sigma, 45345, Oakville, Ontario, Canada), 8 g DDSA (Sigma, 45346, Oakville, Ontario, Canada), 9.5 g MNA (Sigma, 45347, Oakville, Ontario, Canada), 0.25 g DMP-30 (Sigma, 45348, Oakville, Ontario, Canada), the tissue was first washed in 50:50 acetone : resin for 15 min, then in resin twice for 15 min each. The tissue was then embedded in BEEM® embedding capsule (Electron Microscopy Science, 69910, Hatfield, PA, USA) and polymerized overnight at 80°C.

The ultrathin sections (80-100 nm) were mounted on copper grids 300 Mesh No. 100 (Electron Microscopy Science, 191007, Hatfield, PA, USA) and stained with uranyless EM stain (Electron Microscopy Science, 22409, Hatfield, PA, USA) and lead citrate (Electron Microscopy Science, 22410, Hatfield, PA, USA). The sections were viewed using an FEI Tecnai G2 Spirit transmission electron microscope (FEI, Hillsboro, OR) operating at 80KV. Mitochondrial number and morphology, including area (μm^2), perimeter (μm), circularity, length (μm), width (μm), circularity and elongation were measured as previously described

(Lam *et al.* 2021) using ImageJ software (*http://rsbweb.nih.gov.qe2a-proxy.mun.ca/ij/*). Briefly, the area, length and width of mitochondria were outlined and then processed for analysis. NPCs were outlined, and the area (μm^2) and perimeter (μm) were measured using through ImageJ as described by Lam *et al.,* 2021. 12 NPCs per 100nm thick section were imaged for each genotype, and the total mitochondria per cell were measured.

2.10 Statistics

Statistical analysis was conducted using GraphPad PrismV (GraphPad Software, Inc., CA, United States). One way ANOVA was used in the BrdU/EdU pulse assay experiments to compare total % of all BrdU+ cells (BrdU+/total Hoechst+ cells), % single labeled BrdU cells (only BrdU+/total BrdU+ cells) and % double labeled ([BrdU+ & EdU+]/total BrdU+ cells). One way ANOVA was used to measure % apoptotic cells (total number of condensed nuclei/total Hoechst$^+$ cells), and % of apoptotic cells that were single BrdU labeled or double BrdU &EdU labeled. One way ANOVA was used in the Nestin/Tom20 experiments to compare the number of mitochondria per cell in each genotype analyzed. One way ANOVA was used in the EM experiments to compare the number of mitochondria per cell, average area (μm^2), average perimeter (μm), average length (μm), average width (μm), circularity and elongation of mitochondria. One way ANOVA was used to measure the average cell area (μm^2) and perimeter (μm). Tukey's post hoc analysis was performed when main effects were detected with significance assessed at $p < 0.05$.

Chapter 3: Results

3.0 The role of Mcl-1 in developmental neurogenesis

The requirement of Mcl-1 for NPCs survival occurs at E11, the start of neurogenesis, as apoptosis in the MKO developing forebrain is first observed at E11 (Flemmer et al., 2021). As the pattern of apoptosis in the MKO follows the pattern of differentiation, beginning ventrally and spreading dorsally, two regions of the developing brain were examined: a ventral region, the medial ganglionic eminence and a dorsal region, the cortex, at E11.

3.1 Loss of Mcl-1 results in premature differentiation of NPCs in the medial ganglionic eminence

To examine the impact of loss of Mcl-1 on NPCs proliferation and differentiation at the start of neurogenesis in the MGE, a BrdU/EdU assay was performed (Figure 3.1A, B, B'). BrdU was injected in pregnant mice 24 hours prior to sacrifice at E11 to label all proliferating NPCs at this timepoint. EdU was injected on E11, 2 hours prior to sacrifice to label all proliferating NPCs at this timepoint. NPCs that were singly labelled with BrdU represent NPCs that were in the cell cycle on E10 and then exited the cell cycle by E11. NPCs that were double labelled with BrdU and EdU represent NPCs that were in the cell cycle at E10 and were still in the cell cycle at E11 upon sacrifice. A comparison of BrdU+ NPCs revealed that 40%-50% of NPCs were proliferating at E10 across all genotypes analyzed, demonstrating that the number of proliferating NPCs at E10 was comparable (p=0.16) (Figure 3.1C). No significant difference was observed in the total number of Hoechst+ nuclei per counting area in all genotypes analyzed (p=0.67) (Figure 3.1D). Quantification of the number of double labelled BrdU+ and EdU+ NPCs demonstrated that

a mean of 90% of NPCs were double labelled at E11 in control embryos, indicating that the majority of NPCs were still proliferating upon sacrifice at E11 (Figure 3.1E). In contrast, only 55% of NPCs were double labelled in the MKO ($p<0.0001$) (Figure 3.1E). The MKO:BaxKO genotype rescued the observed phenotype of MKO embryos, as 90% of NPCs double labelled for BrdU+ and EdU+ (Figure 3.1E). The BaxN genotype was comparable to the control and MKO:BaxKO phenotypes, with 90% of NPCs were double labelled for BrdU+ and EdU+ (Figure 3.1E). Analysis of NPCs that were only labelled with BrdU+ revealed that approximately 10% of the total BrdU+ NPC population had exited the cell cycle by E11 (Figure 3.1F). In contrast, a significant increase in single-labeled BrdU+ NPCs was observed in the MKO, with a mean of 45% of cells single-labelled with BrdU ($p<0.0001$) (Figure 3.1F). The MKO:BaxKO genotype rescued the observed phenotype of MKO embryos, as 10% of NPCs were single labelled for BrdU (Figure 3.1F). The BaxN genotype was comparable to the control and MKO:BaxKO (Figure 3.1F). These results demonstrate that NPCs in the medial ganglionic eminence of the MKO prematurely exited the cell cycle.

NPCs apoptosis within the medial ganglionic eminence was examined next through quantifying condensed nuclei. In littermate controls, apoptosis was not observed at E11. Apoptosis was observed in MKOs only with a mean of 15% of cells (46 NPCs/counting area) ($p<0.0001$) (Figure 3.1G). Apoptosis was not observed in the MGE of MKO:BaxKO forebrain, indicating that NPCs were rescued from an apoptotic fate. The BaxN genotype was comparable to the control and MKO:BaxKO phenotypes as apoptosis was not observed in the NPC population.

The sex of the embryos was included in the descriptive data points. Although there were insufficient samples from male and female tissue for statistical analysis, the data points appeared comparable (Figure 3.1C-H).

Taken together, the results of this experiment demonstrate that loss of Mcl-1 results in premature neurogenesis in the MKO developing forebrain at E11, with apoptosis primarily occurring within NPCs that had exited the cell cycle at this timepoint.

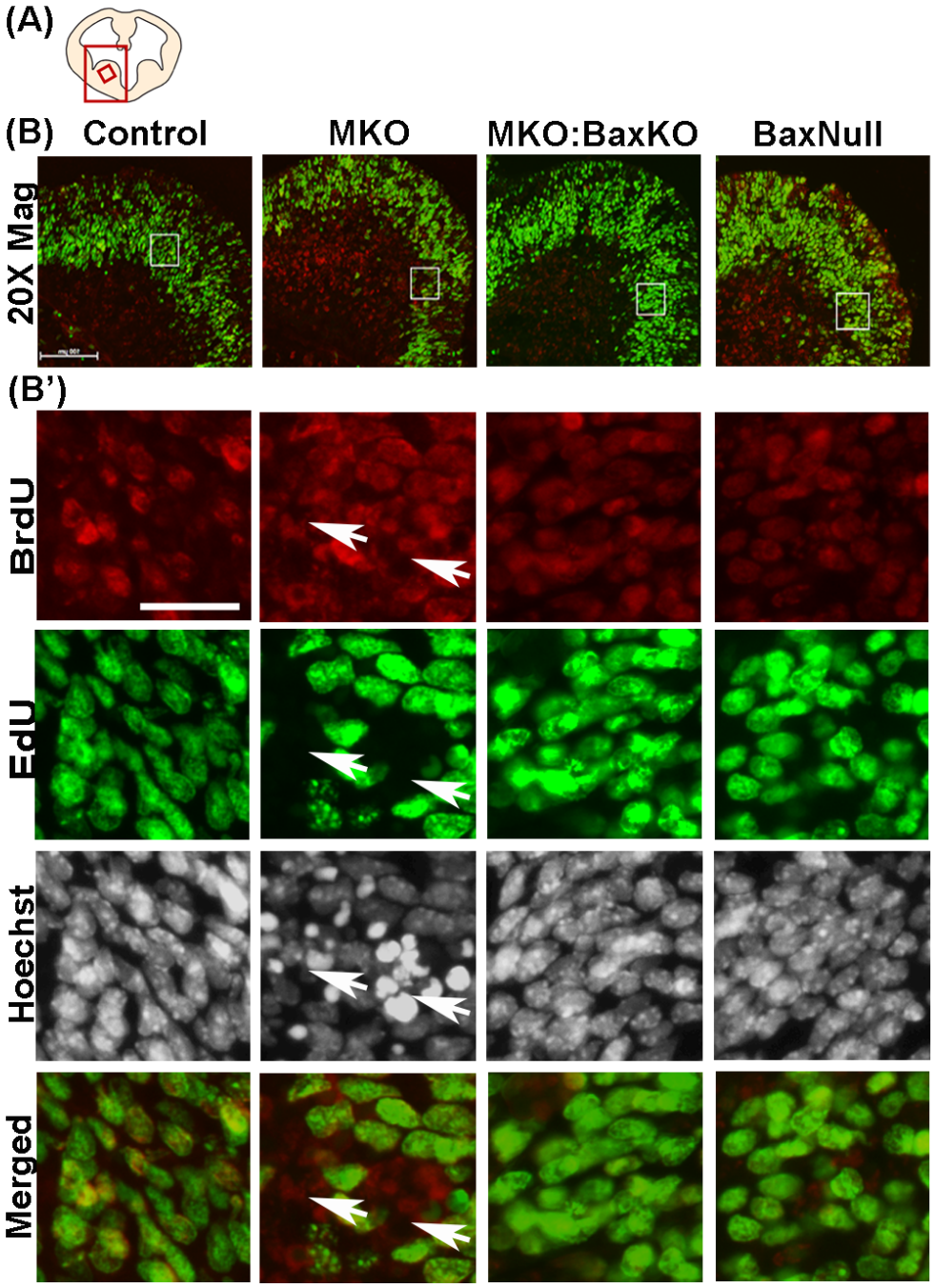
(A)
(B)
Control
MKO
MKO:BaxKO
BaxNull
20X Mag
(B')
BrdU
EdU
Hoechst
Merged

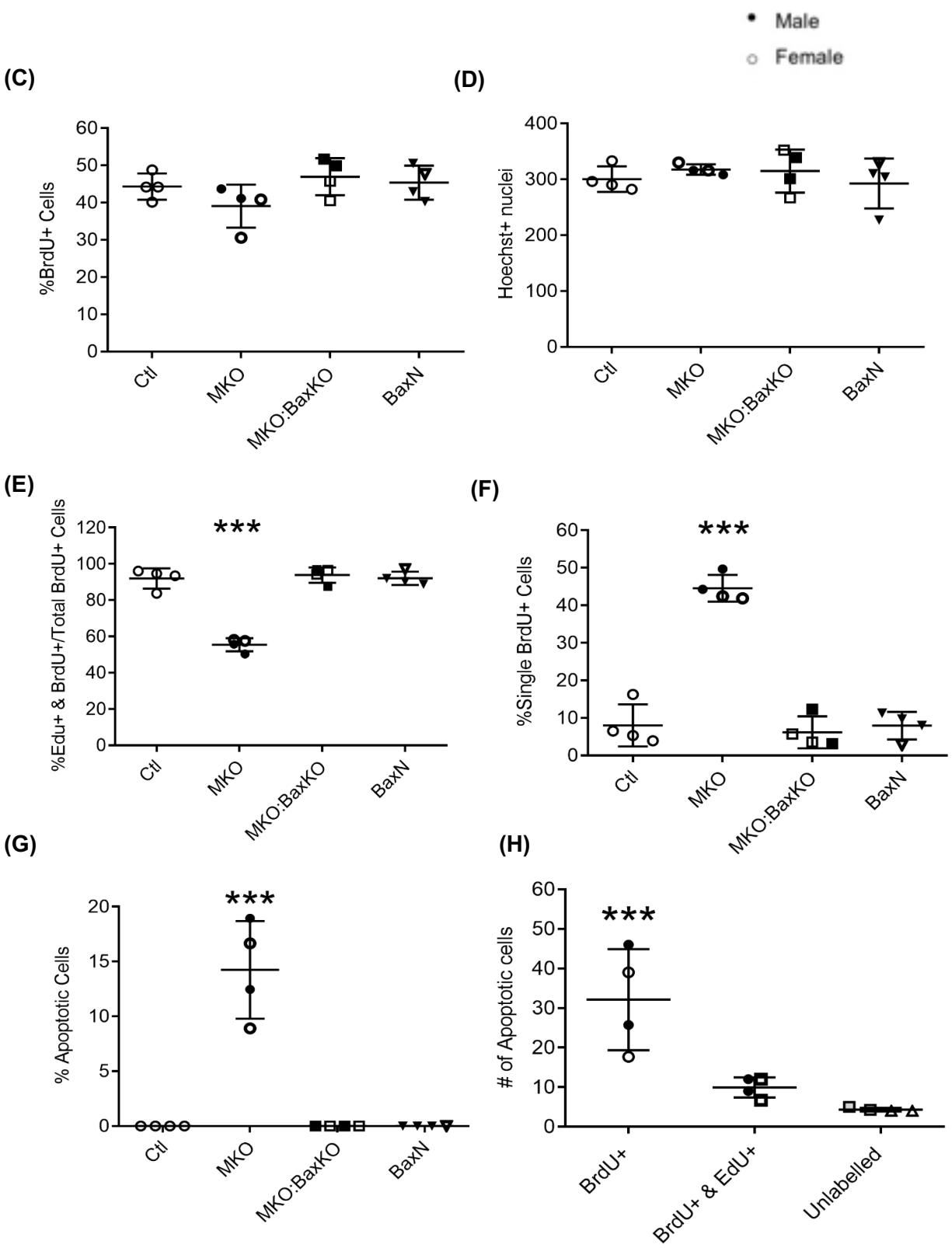
(C)
(D)
Male
Female
%BrdU+ Cells
Hoechst+ nuclei
Ctl
MKO
MKO:BaxKO
BaxN
(E)
(F)
%Edu+ & BrdU+/Total BrdU+ Cells
%Single BrdU+ Cells
***
(G)
(H)
% Apoptotic Cells
# of Apoptotic cells
BrdU+
BrdU+ & EdU+
Unlabelled

Figure 3.1: MKO NPCs prematurely exit the cell cycle in the medial ganglionic eminence at the onset of neurogenesis. (A) Line drawings of a coronal section through the brain of an E11 embryo with the large red box over the medial ganglionic eminence and the smaller box corresponding to the region where cell counts were performed. (B) Representative low magnification photomicrographs of coronal sections double labelled for BrdU and EdU. Scale bar = 100 μm. (B') Higher magnification images of boxed areas in B labelled for BrdU (red), EdU (green) and Hoechst (white). Scale bar = 20 μm. All cell counts were performed within a 200 μm by 100 μm boxed area within the MGE. (C) The percent of BrdU+ NPCs of the total number of Hoechst + nuclei. (D) Total number of Hoechst + NPCs per counting area. (E) The percent of proliferating NPCs (BrdU+ and EdU+) (F) The percent of differentiating NPCs (BrdU+). (G) The percent of apoptotic NPCs. (H) The number of apoptotic cells labelled BrdU+, BrdU+ & EdU+ or unlabelled in the MKO. Arrows indicate apoptotic NPCs. Solid symbols = male embryos, open symbols = female embryos. One-way ANOVA was performed on the means of all groups followed by Tukey's multiple comparison test. CTL (n = 5), MKO (n = 4), MKO:BaxKO (n = 4) and BaxNull (n=4). ***$p < 0.001$, error bars represent ± SD.

3.2 Loss of Mcl-1 results in premature differentiation of NPCs in the developing cortex

Premature cell cycle exit in response to loss of Mcl-1 was observed in the medial ganglionic eminence where neurogenesis first initiates at E11. Therefore, the dorsal cortex was examined next to determine whether loss of Mcl-1 similarly resulted in premature differentiation of NPCs throughout the developing forebrain (3.2A, B, B'). An analysis of the total number of BrdU+ NPCs in all genotypes revealed that approximately 50% of NPCs were proliferating at E10 (p=0.23) (Figure 3.2C). No significant difference in total Hoechst+ nuclei was observed, demonstrating that this region was comparable amongst all genotypes for analysis (p=0.63) (Figure 3.2D). Quantification of the number of double labelled BrdU+ and EdU+ NPCs revealed that approximately 90% of the BrdU+ NPCs population were proliferating upon sacrifice at E11 (Figure 3.2E). In contrast, 85% of NPCs were BrdU+ and EdU+ in MKO embryos (p=0.0031) (Figure 3.2E). The MKO:BaxKO genotype rescued the observed phenotype of MKO embryos, as 90% of NPCs were double labelled (Figure 3.2E). The percentage of double labelled NPCs in the BaxN genotype was comparable to the control and MKO:BaxKO embryos (Figure 3.2E). Analysis of NPCs that were only labelled with BrdU revealed that 10% of NPCs had exited the cell cycle by E11 in littermate controls (Figure 3.2F). Conversely, 15% of NPCs were single labelled with BrdU in MKO embryos (p=0.0031) (Figure 3.2F). The MKO:BaxKO genotype rescued the observed phenotype of MKO embryos, as 10% of NPCs were single labelled for BrdU+ (Figure 3.2F). The BaxN genotype was comparable to control and MKO:BaxKO embryos (Figure 3.2F). Ultimately, premature differentiation of the NPCs population was observed in the MKO developing cortex.

Next, apoptotic cell death was compared across genotypes. In littermate controls, approximately 1% of NPCs underwent apoptosis upon sacrifice at E11 (Figure 3.2G). In contrast approximately 8.7% of NPCs (14 NPC/counting area) were apoptotic in the MKO developing cortex upon sacrifice ($p<0.0001$). Apoptosis was not observed in the developing cortex of MKO:BaxKO embryos, indicating that NPCs were rescued from an apoptotic fate. The BaxN genotype was comparable to the control and MKO:BaxKO phenotype as apoptosis was not observed in the NPCs population.

Next, to determine whether apoptosis was occurring in the proliferative or differentiative NPCs population in MKO embryos, the BrdU and EdU labelled NPCs were examined. Apoptosis was primarily occurring in the proliferative NPCs population, as a mean of 11 apoptotic cells per counting area were both BrdU+ and EdU+ ($p<0.0001$) (Figure 3.2H). A mean of 3 apoptotic cells per counting area labelled with BrdU+ only indicating they had exited the cell cycle, while a mean of 2 apoptotic NPCs per counting area were unlabelled.

The sex of the embryos was included in the descriptive data points. Although there were insufficient samples from male and female tissue for statistical analysis, the data points appeared comparable (Figure 3.2C-H).

Taken together, the results of this experiment demonstrate that loss of Mcl-1 results in premature neurogenesis in the developing cortex at E11, with apoptosis primarily occurring within the proliferative cell population at this timepoint.

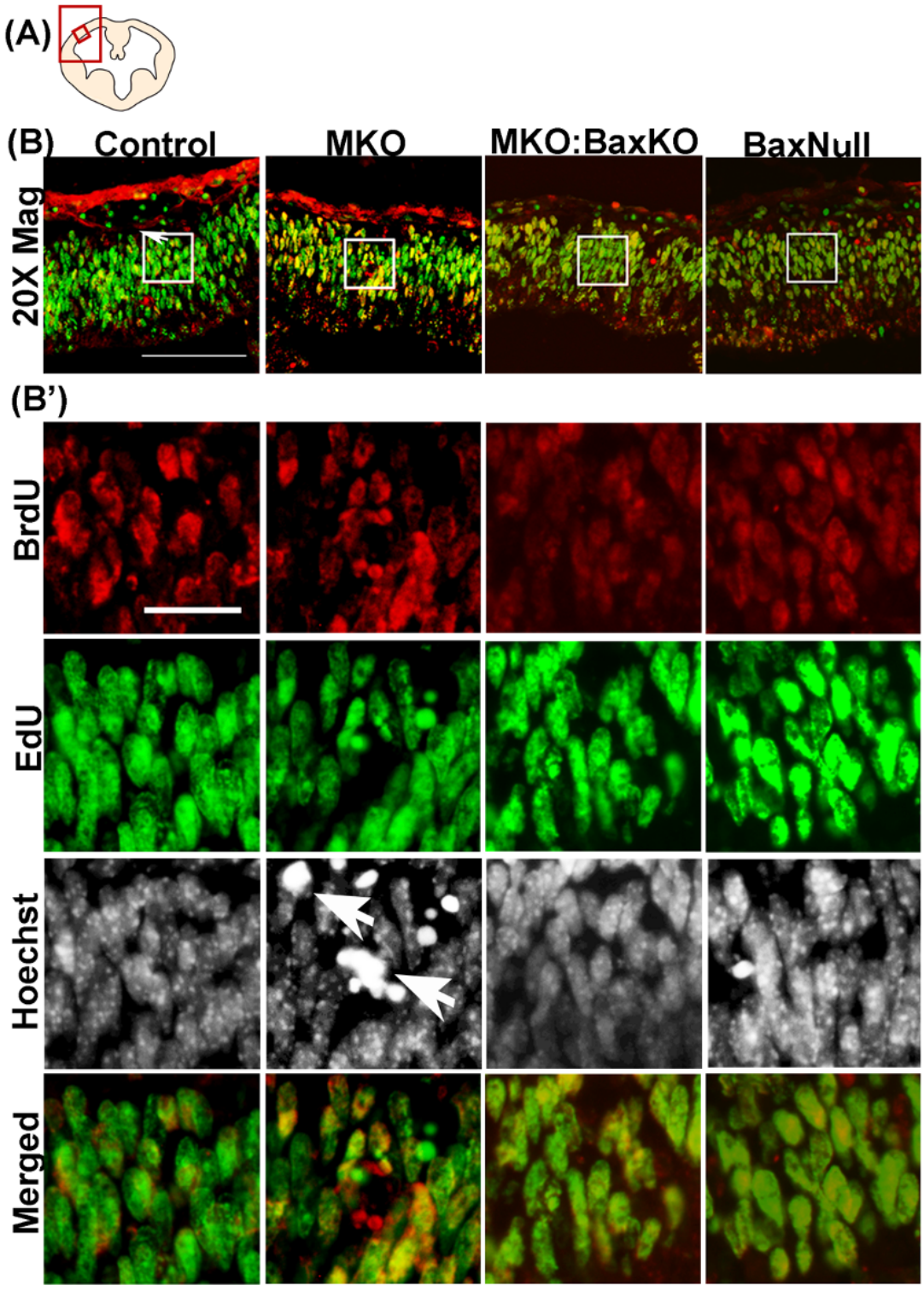
(A)
(B)
Control
MKO
MKO:BaxKO
BaxNull
20X Mag
(B')
BrdU
EdU
Hoechst
Merged

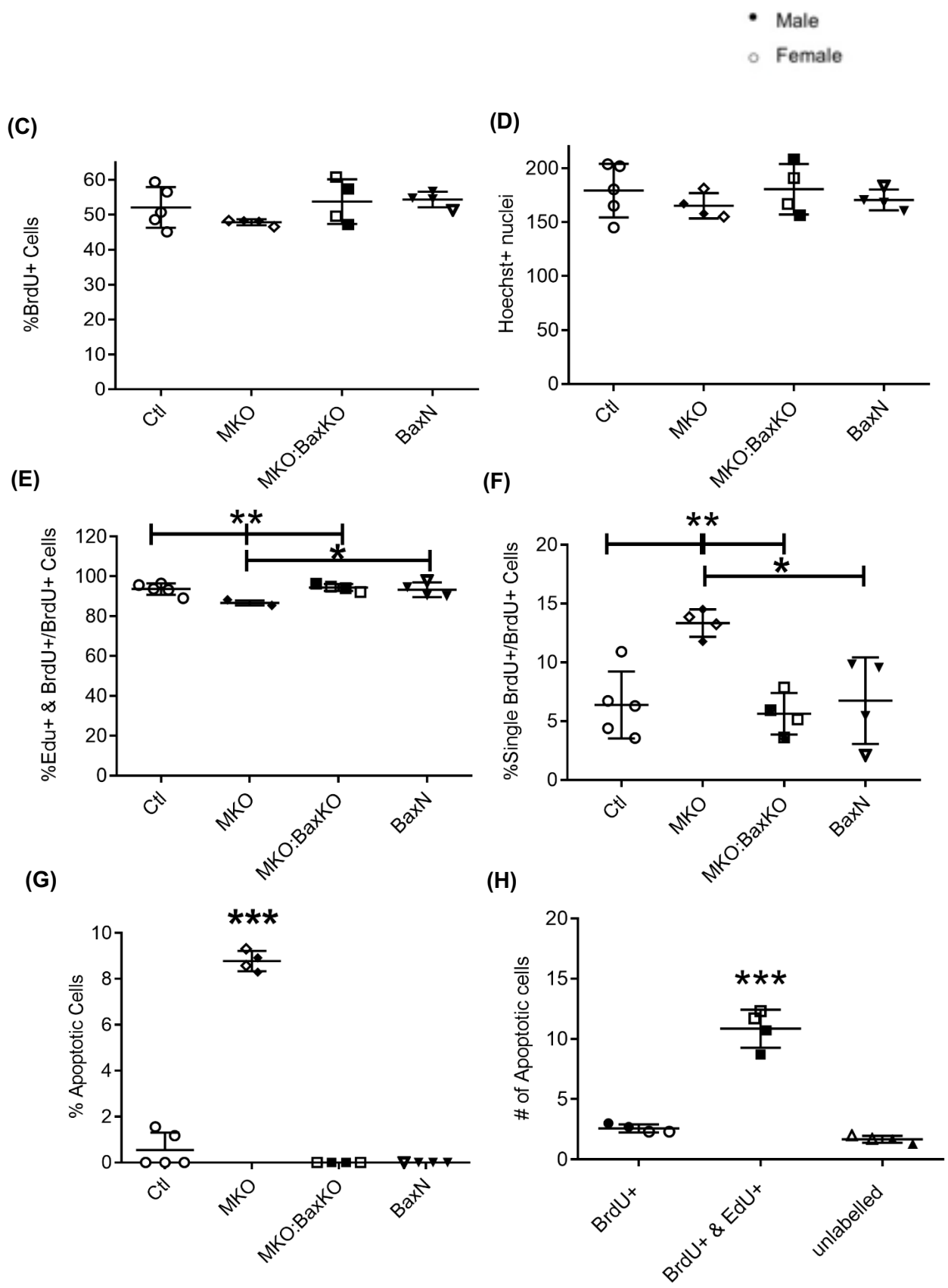
Male
Female
(C)
%BrdU+ Cells
0
10
20
30
40
50
60
Ctl
MKO
MKO:BaxKO
BaxN
(D)
Hoechst+ nuclei
0
50
100
150
200
Ctl
MKO
MKO:BaxKO
BaxN
(E)
%Edu+ & BrdU+/BrdU+ Cells
0
20
40
60
80
100
120
**
*
Ctl
MKO
MKO:BaxKO
BaxN
(F)
%Single BrdU+/BrdU+ Cells
0
5
10
15
20
**
*
Ctl
MKO
MKO:BaxKO
BaxN
(G)
% Apoptotic Cells
0
2
4
6
8
10
***
Ctl
MKO
MKO:BaxKO
BaxN
(H)
# of Apoptotic cells
0
5
10
15
20
***
BrdU+
BrdU+ & EdU+
unlabelled

Figure 3.2: MKO NPCs prematurely exit the cell cycle in the developing cortex at the onset of neurogenesis. (A) Line drawings of a coronal section through the brain of an E11 embryo with the large red box indicating the cortex and the smaller red box corresponding to the region where cell counts were performed. (B) Representative low magnification photomicrographs of coronal sections double labelled for BrdU and EdU. Scale bar = 100 µm. (B') Higher magnification images of boxed areas in B labelled for BrdU (red), EdU (green) and Hoechst (white). Scale bar = 20 µm. All cell counts were performed within a 100 µm by 200 µm boxed area within the MGE. (C) BrdU+ NPCs represented as a percentage of the total number of Hoechst + nuclei per counting area. (D) Total number of Hoechst + NPCs. (E) The percent of proliferating NPCs (BrdU+ and EdU+). (F) The percent of differentiating NPCs (BrdU+). (G) The percent of apoptotic NPCs. (H) The number of apoptotic cells that are BrdU+, BrdU+ & EdU+ or unlabelled in the MKO. Arrows indicate apoptotic NPCs. Solid symbols = male embryos, open symbols = female embryos. One-way ANOVA was performed on the means of all groups followed by Tukey's multiple comparison test. CTL (n = 5), MKO (n = 4), MKO:BaxKO (n = 4) and BaxNull (n=4). ***$p < 0.001$, **$p < 0.01$, *$p < 0.05$ error bars represent ± SD.

3.3 Loss of Mcl-1 results in more mitochondria in NPCs at the onset of neurogenesis as quantified by NanoJ SRRF

As premature differentiation was observed in MKO NPCs (Figure 3.1, 3.2), the following experiments aimed to determine whether loss of Mcl-1 impacts mitochondrial number in NPCs at the onset of developmental neurogenesis. A Nestin/Tom20 immunohistochemistry was performed on forebrain tissue sections from the MKO developing forebrain, and the number of mitochondria per NPCs was quantified using SRRF analysis (Figure 3.3A, A'). An average of 5 mitochondria per NPCs was observed in the littermate controls (Figure 3.3B). An average of 10 mitochondria per NPCs was observed in the MKO MGE ($p<0.0001$) (Figure 3.3B). The MKO:BaxKO genotype rescued the observed phenotype of MKO embryos, as an average of 6 mitochondria per NPCs was observed (Figure 3.3B). The average number of mitochondria per NPCs in the BaxN genotype was comparable to the control and MKO:BaxKO embryos (Figure 3.3B). Next, parameters of mitochondria morphology including area (μm^2) ($p=0.27$), perimeter (μm) ($p=0.52$), circularity ($p=0.93$) and elongation ($p=0.86$) were examined. No differences in these parameters were observed across all genotypes analyzed (Figure 3.3C-F).

To determine whether MKO cells were larger and therefore had more mitochondria, NPCs morphology was assessed. Comparisons of mitochondrial area (μm^2) ($p=0.066$) and perimeter (μm) ($p=0.28$), revealed no significant differences across all genotypes analyzed (Figure 3.4A, B). The data points for male and female embryos appeared comparable across genotypes (Figure 3.3B-F, Figure 3.4A,B). Taken together, these results demonstrate that conditional deletion of Mcl-1 results in more mitochondria in NPCs at the onset of neurogenesis.

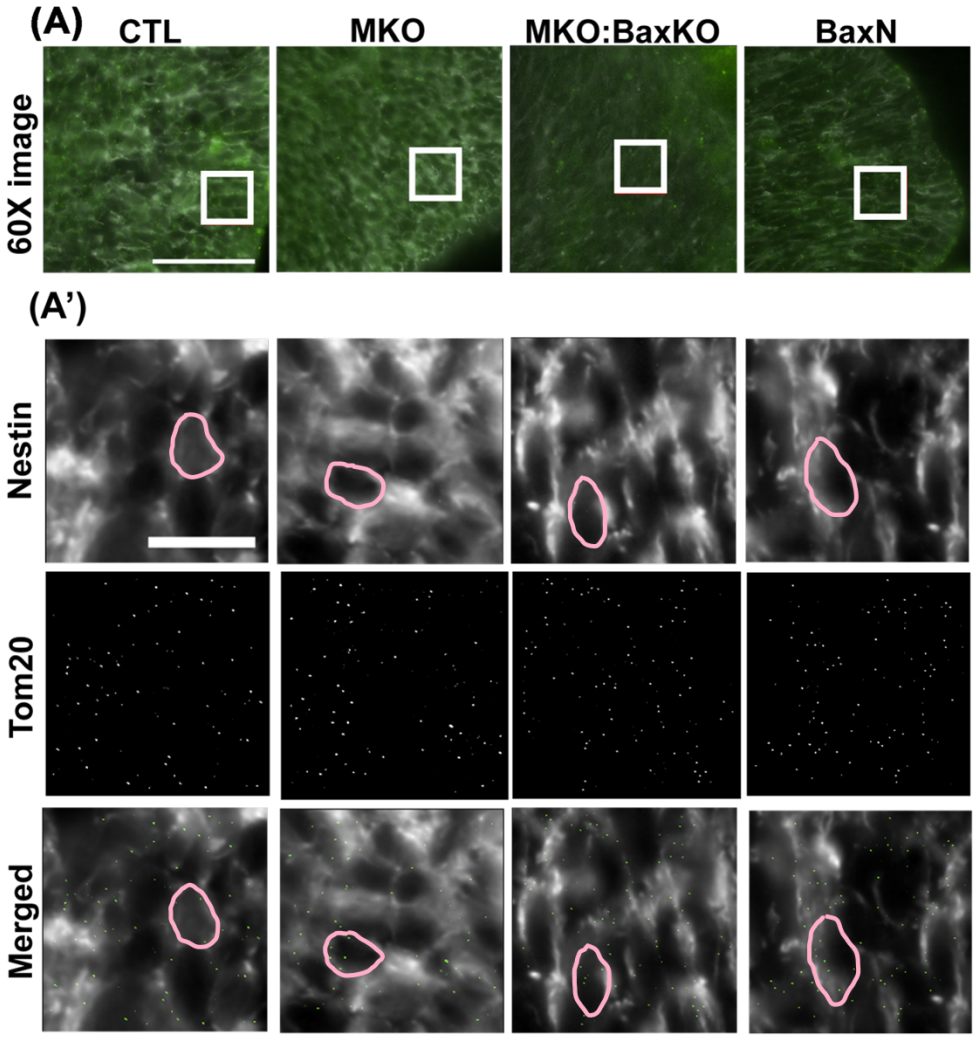
(A)
CTL
MKO
MKO:BaxKO
BaxN
60X image
(A')
Nestin
Tom20
Merged

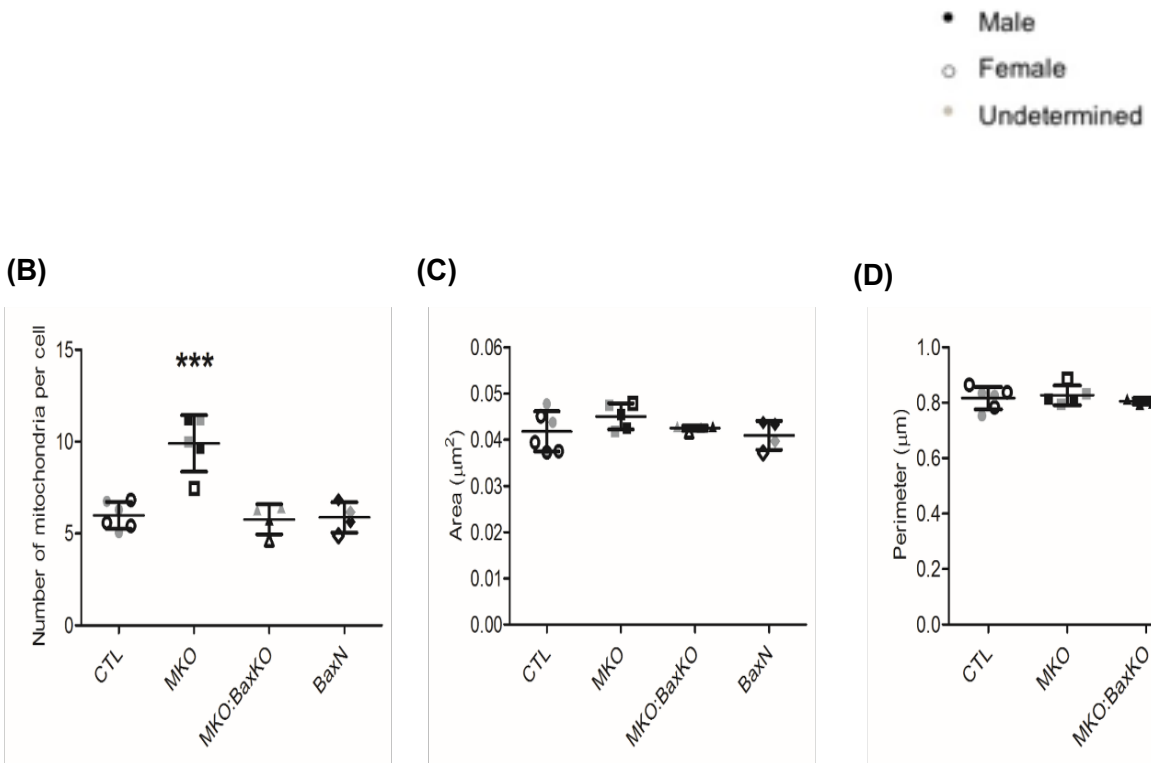
Male
Female
Undetermined
(B)
Number of mitochondria per cell
***
CTL
MKO
MKO:BaxKO
BaxN
(C)
Area (μm²)
(D)
Perimeter (μm)
(E)
Circularity
(F)
Elongation

Figure 3.3: MKO NPCs contain more mitochondria at the onset of neurogenesis. (A) Representative image of Nestin/Tom20 immunohistochemistry in coronal sections in CTL, MKO, Mcl-1:Bax KO, and BaxNull tissue. Scale bar = 50 µm. (A') Higher magnification representative images of boxed areas in B labelled for Nestin (grey), Tom20 after NanoJ SRRF processing (green) and merged images. Individual NPCs are outlined in pink. Scale bar = 10 µm. (B) The number of mitochondria per NPCs was analyzed in 12 cells per embryo. (C-F). (C) The average mitochondrial area (μm^2) (D) perimeter (µm) (E) circularity (F) elongation. Solid symbols = male embryos, open symbols = female embryos, grey symbol = undetermined sex. One-way ANOVA was performed on the means followed by Tukey's multiple comparison test. CTL (n = 6), MKO (n = 5), MKO:Bax KO (n = 4) and BaxNull (n=4). ***$p < 0.001$, error bars represent ± SD.

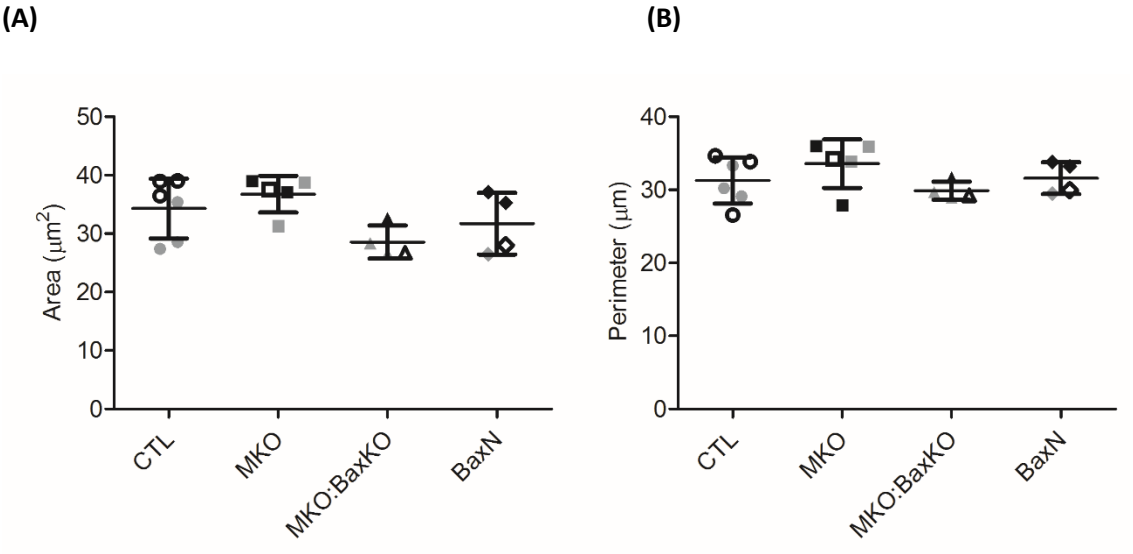

Figure 3.4: Comparable NPCs area and perimeter at the onset of neurogenesis. (A) The average NPCs area (μm^2) and (B) the average NPCs perimeter (μm). Solid symbols = male embryos, open symbols = female embryos, grey symbol = undetermined sex. One-way ANOVA was performed on the means followed by Tukey's multiple comparison test. CTL (n = 6), MKO (n = 5), MKO:Bax KO (n = 4) and BaxNull (n=4). ***$p < 0.001$, error bars represent ± SD.

3.4 Loss of Mcl-1 results in more mitochondria in NPCs at the onset of neurogenesis as quantified through electron microscopy

As more mitochondria were observed in NPCs with Nestin/Tom20 immunohistochemistry (Figure 3.3), electron microscopy of NPCs was performed to validate this finding. The medial ganglionic eminence of E11 MKOs and control littermates were dissected and processed for electron microscopy (Figure 3.5A). Similar to the Nestin/Tom20 results, an average of 6 to 7 mitochondria per NPCs per section was observed in wild type and Mcl-1 heterozygote (HET) littermate controls, respectively (Figure 3.5B). In contrast, approximately 10 mitochondria per NPCs was observed in the MKO (p=0.0036) (Figure 3.5B). Next, parameters of mitochondria morphology including area (μm^2) (p=0.4475), perimeter (μm) (p=0.2182), length (μm) (p=0.2088), width (μm) (p=0.4738), circularity (p=0.1457) and elongation (p=0.1346) were examined. No differences in these parameters were observed across all genotypes analyzed (Figure 3.5C-H).

An analysis of NPCs morphology, including area (μm^2) and perimeter (μm) was conducted. No difference in average NPCs area (p=0.5326) or perimeter (p=0.4049) were observed across all genotypes (Figure 3.6A,B). The sex of the embryos was indicated for each data point and revealed that the data from male and female embryos were comparable across all genotypes (Figure 3.5C-H, Figure 3.6A,B). Taken together, these results demonstrate that conditional deletion of Mcl-1 results in greater number of mitochondria per NPCs, but no alterations in mitochondrial morphology or NPCs size and shape during developmental neurogenesis in the medial ganglionic eminence at E11.

(A)

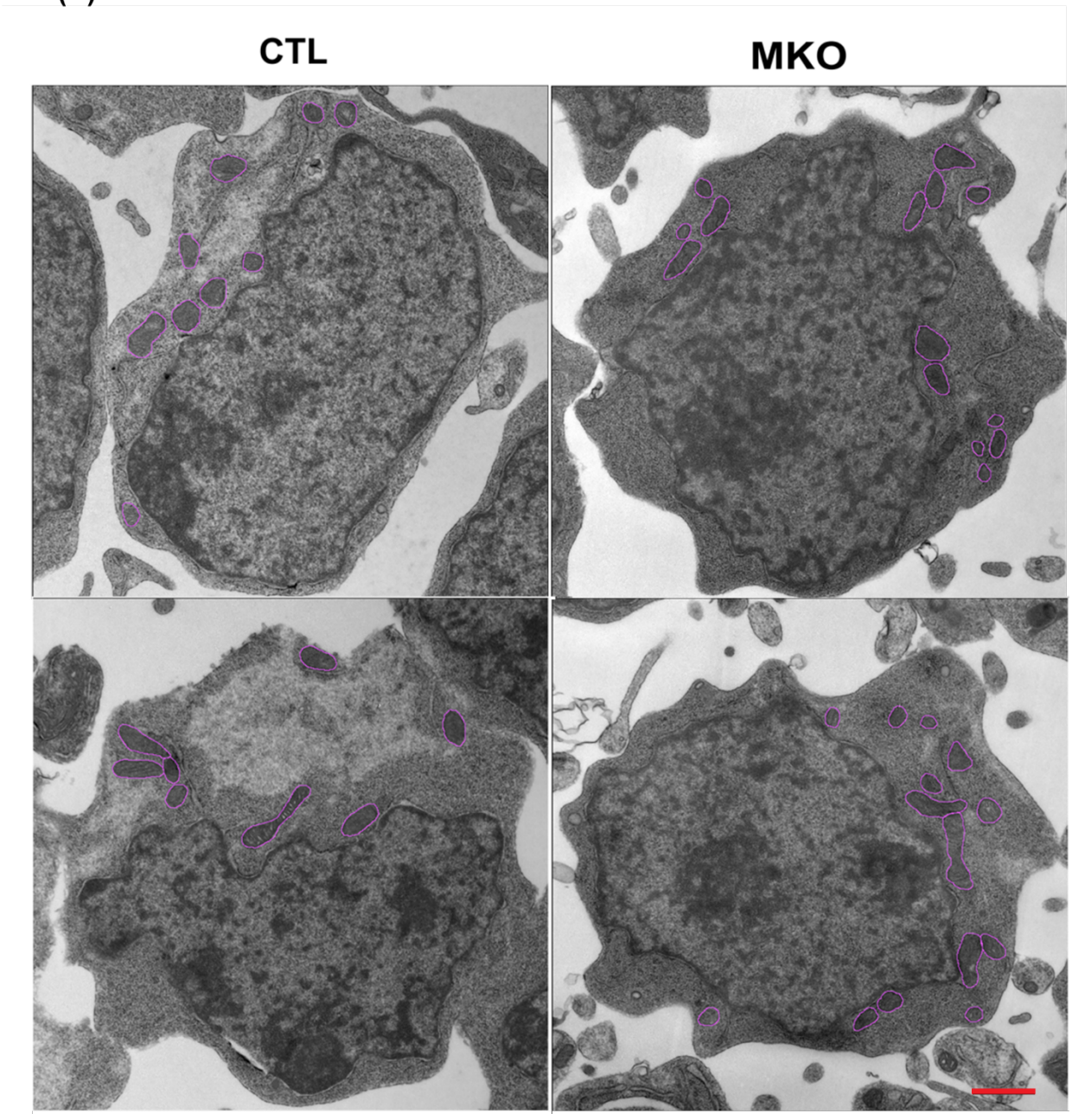

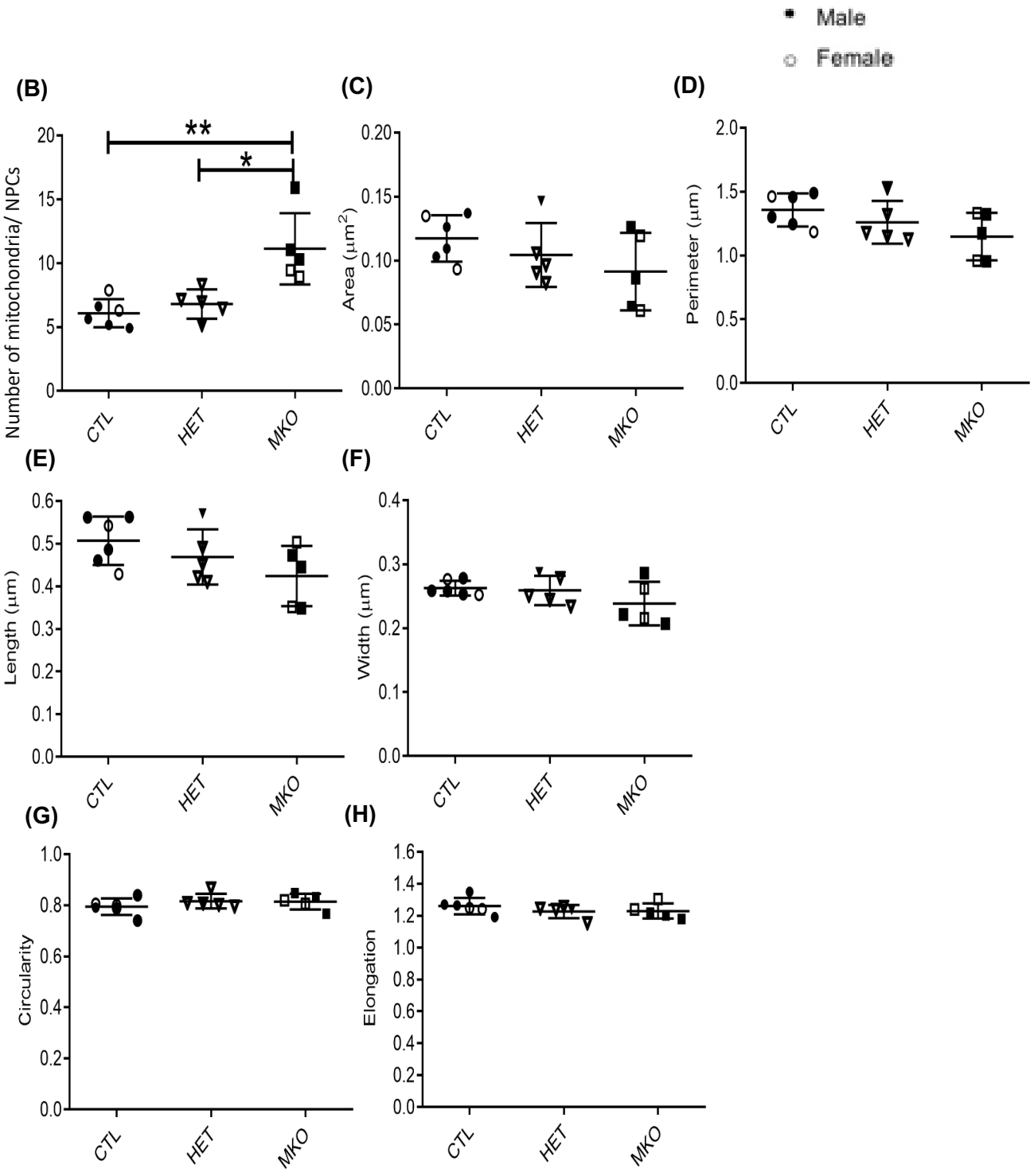
Male
Female
(B)
(C)
(D)
Number of mitochondria/ NPCs
Area (μm2)
Perimeter (μm)
**
*
CTL
HET
MKO
(E)
(F)
Length (μm)
Width (μm)
(G)
(H)
Circularity
Elongation

Figure 3.5: Increased mitochondria per NPCs in the MKO medial ganglionic eminence. (A) Representative images of mitochondria per NPCs in MKO, HET and littermate controls. Mitochondria are outlined in purple. Scale bar = 800 μm. (B) The number of mitochondria per NPCs was analyzed in 12 cells per embryo. (C-F) Mitochondrial measurements. (C) The average mitochondrial area (μm^2), (D) perimeter (μm), (E) length (μm), (F) width (μm), (F) circularity and (G) elongation per NPCs. One-way ANOVA was performed on the means followed by Tukey's multiple comparison test. Solid black symbols = male embryos, open symbols = female embryos. CTL (n = 5), MKO (n = 5), HET (n = 5). $^{**}p < 0.01$, $^{*}p<0.05$, error bars represent ± SD.

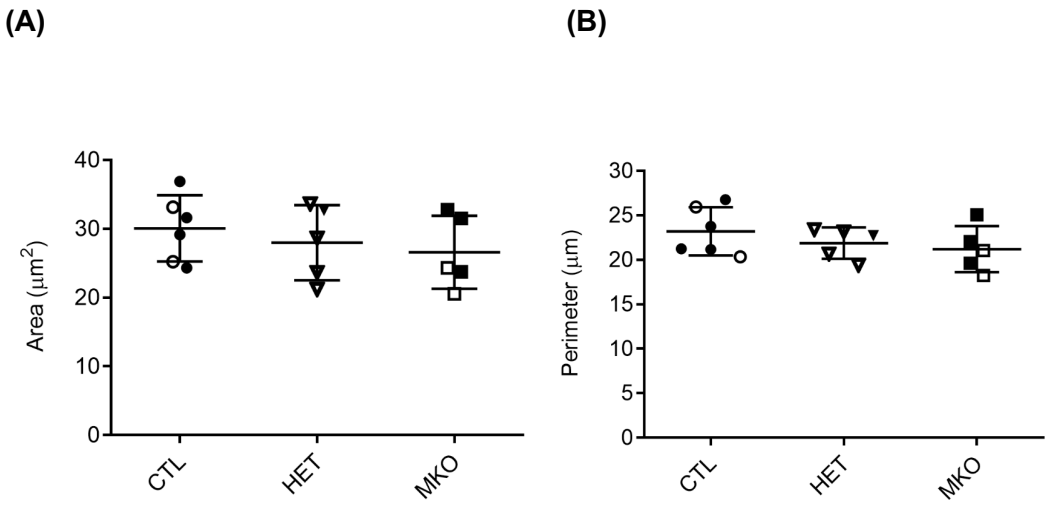

Figure 3.6: Comparable NPCs area and perimeter at the onset of neurogenesis. (A) The average NPCs area (μm^2) and (B) the average NPCs perimeter (µm). Solid symbols = male embryos, open symbols = female embryos. One-way ANOVA was performed on the means followed by Tukey's multiple comparison test. CTL (n = 5), MKO (n = 5), HET (n = 5) error bars represent ± SD.

3.5 Nestin/Tom20 IHC with NanoJ SRRF processing is comparable to EM analysis for mitochondrial number and morphological measurements.

Mitochondrial number and morphology were examined using two distinct methods: Nestin/Tom20 IHC with NanoJ SRRF processing and EM analysis (Figures 3.3, 3.5). To date, Nestin/Tom20 IHC with NanoJ SRRF processing has not been used to measure mitochondrial number or morphology and therefore is a novel technique for this application. In order to validate the results from the Nestin/Tom20 with NanoJ SRRF processing, mitochondrial number and morphology were measured through EM analysis. Mitochondrial number and morphological measurements from each analysis were compared (Figure 3.7). Both analyses found comparable numbers for mitochondrial number (p=0.65), circularity (p=0.74), elongation (p=0.85) and NPCs area (p=0.051) (Figure 3.7A,B,C,D). Therefore, it was determined that Nestin/Tom20 IHC with NanoJ SRRF processing is a comparable technique to measure mitochondrial number and morphology.

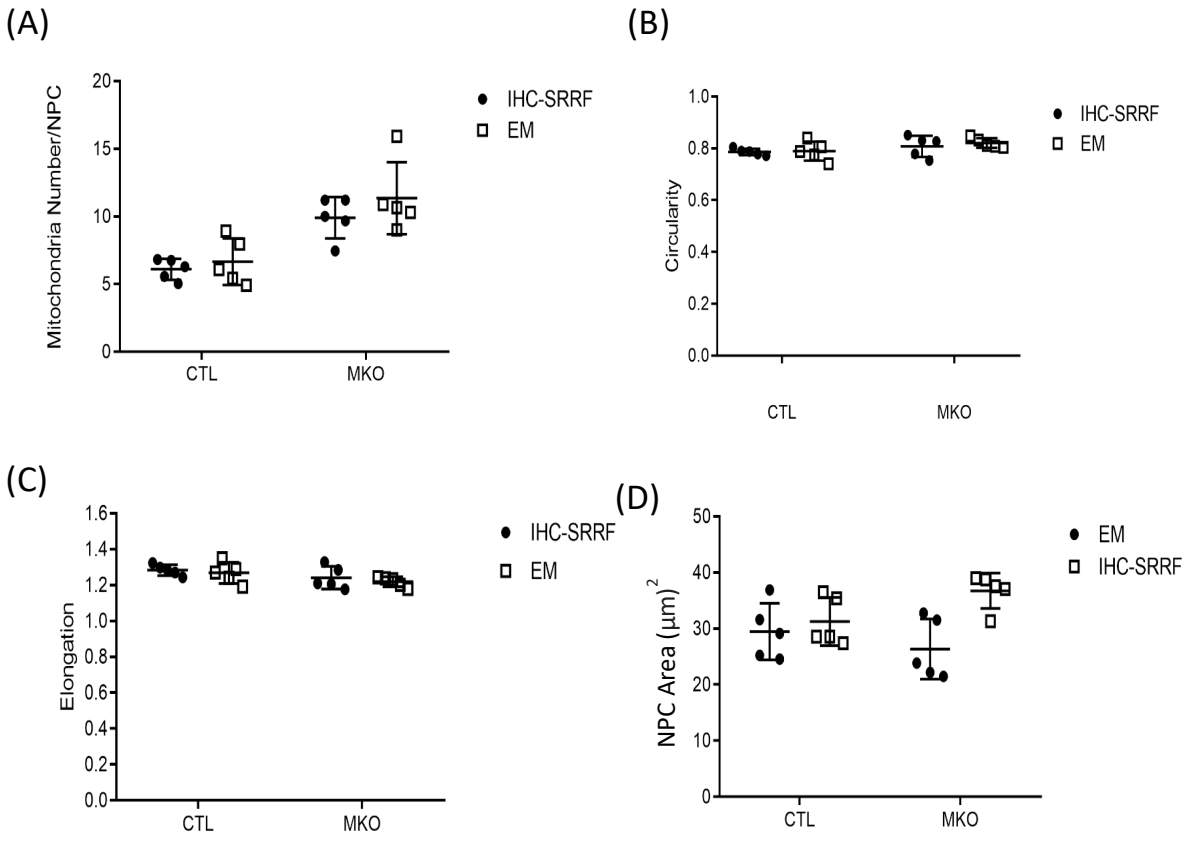

Figure 3.7: Nestin/Tom20 IHC with NanoJ SRRF processing is a comparable technique to measure mitochondrial number and morphology. Mitochondrial number and morphology were measured through IHC with NanoJ SRRF processing and EM (A) The number of mitochondria per NPCs. (B) circularity and (C) elongation per NPCs. (D) The average NPCs area (μm^2). Two-way ANOVA was performed on the means followed by Bonferroni's multiple comparison test. Solid black symbols = male embryos, open symbols = female embryos. CTL (n = 5), MKO (n = 5). Error bars represent ± SD.

Chapter 4: Discussion

These studies identifies four novel findings elucidating the role of Mcl-1 within the developing murine CNS. Specifically, this thesis focused on the role of Mcl-1 at the onset of neurogenesis using conditional loss-of-function experiments within the developing murine CNS. First, it demonstrates that loss of Mcl-1 in NPCs results in premature cell cycle exit at the onset of neurogenesis, with a percentage of these NPCs undergoing apoptosis. Second, it shows through both IHC and EM analysis that loss of Mcl-1 results in an increase in the number of mitochondria within NPCs at the onset of neurogenesis. Third, the observed effects of loss of Mcl-1 on cell cycle exit and mitochondrial number are rescued in MKO: BaxKO embryos indicating an interaction of Mcl-1 and Bax in these processes during developmental neurogenesis. Finally, this thesis establishes the use of Nestin/Tom20 IHC with NanoJ SRRF processing as a comparable technique to EM to assess mitochondrial number and size. Taken together, these results demonstrate an additional role of Mcl-1 in the survival of NPCs at the onset of neurogenesis.

4.1 Mcl-1 mediates NPCs cell cycle exit and survival at the onset of neurogenesis

These studies examines cell cycle exit at the onset of neurogenesis in two different regions of the developing forebrain: the MGE and the dorsal cortex. Both areas were selected for analysis as neurogenesis progresses from ventral to dorsal in the developing forebrain. Prior to the onset of neurogenesis at E10 roughly 50% of NPCs were proliferating in each region. At the onset of neurogenesis at E11 approximately 90% of the NPCs that were labelled with BrdU at E10 were still in the cell cycle in both the MGE and cortex. Furthermore, a comparable percentage of BrdU+ NPCs had exited the cell cycle in both

regions, with approximately 8% and 6% of NPCs exiting the cell cycle in the MGE and dorsal cortex, respectively. Due to the path of differentiation, it was expected that more NPCs would exit the cell cycle in the MGE in comparison to the dorsal cortex. The observed results could be in part due to slight variations in the gestation period of pregnant mice. Pregnancy was determined through the detection of a vaginal plug in female mice, which were checked for once in the morning and afternoon. Checking for pregnancy at these timepoints therefore may lead to variations in the gestation period of pregnant mice, with some mice further along their gestation period than others. Though BrdU and EdU were injected at E10 and E11 respectively, the variations in gestation period may result in the onset of neurogenesis not fully being captured. Increasing the sample size of embryos would therefore need to be performed in future. Premature cell cycle exit was observed in MKOs at the onset of neurogenesis. In contrast to the results of littermate controls, the rate of cell cycle exit in response to loss of Mcl-1 varied in each region of the developing forebrain analyzed. Loss of Mcl-1 resulted in half of the BrdU+ NPCs undergoing premature cell cycle exit in the MGE. In contrast, loss of Mcl-1 in the developing cortex resulted in 15% of BrdU+ NPCs undergoing premature cell cycle exit. The observed differences in NPCs cell cycle exit in each region is in concordance with the path of differentiation, as a greater percentage of cell cycle exit occurs ventrally. Mcl-1 is required for the survival of NPCs at the onset of neurogenesis (Fogarty et al., 2019). Furthermore, Mcl-1 has an established role in cell cycle exit and differentiation (Harley et al., 2010; Hasan et al., 2013; Kozopas et al., 1993; Rinkenberger et al., 2000). In concordance with these studies, this thesis demonstrates that Mcl-1 plays a role in NPCs cell cycle exit occurring in tandem with the path of differentiation.

These studies examined the percentage of apoptosis in both the MGE and dorsal cortex. In littermate controls, a minimal percent of NPCs underwent apoptosis, with no NPCs and 1% of NPCs undergoing apoptosis in the MGE and dorsal cortex respectively. Apoptosis was observed in the MGE and dorsal cortex of MKO embryos, with the number of apoptotic NPCs varying in each region. A greater number of NPCs underwent apoptosis in the MGE in comparison to the dorsal cortex, as approximately 46 NPCs underwent apoptosis in the MGE in comparison to 14 NPCs in the dorsal cortex. The majority of apoptosis in the MGE occurred in NPCs that had exited the cell cycle, equating to approximately 30 BrdU+ NPCs. In contrast, only 3 BrdU+ NPCs apoptosis in the dorsal cortex at this time point,. Importantly, the number of proliferating (BrdU+ and EdU+) NPCs that underwent apoptosis did not vary between each region, as 10 and 11 NPCs were observed in the MGE and dorsal cortex respectively. Thus, the increased apoptosis observed in the MGE was a result of NPCs that prematurely exited the cell cycle in response to loss of Mcl-1. These results demonstrate the dependence of NPCs on Mcl-1 for survival upon differentiation. Previous studies have established that Mcl-1 is required for the survival of NPCs at the onset of neurogenesis, as conditional deletion of Mcl-1 in the CNS results in apoptosis occurring in the developing forebrain at E11 (Fogarty et al., 2019; Flemmer et al., 2021). Cell-type-specific labeling was not performed in this thesis to determine if the NPCs that had exited the cell cycle prematurely differentiated. However, previous research has demonstrated that apoptotic cells in MKO were labeled with Nestin antibodies, doublecortin, a neuroblast marker, or βIII tubulin-1, an immature neuronal marker (Arbour et al., 2008). These findings demonstrate that NPCs die during the process of differentiation into immature neurons in the MKO developing forebrain. Furthermore, the progression of apoptosis in

MKOs follows the path of differentiation spreading from ventral to dorsal (Flemmer et al., 2021; Gouti et al., 2015). The observed differences in the rates of apoptosis of this thesis further demonstrate that the dependence of NPCs on Mcl-1 for survival occurs upon differentiation.

4.2 Mcl-1 regulates mitochondrial number in NPCs at the onset of neurogenesis

The results of these studies demonstrated that loss of Mcl-1 results in an increased number of mitochondria per NPCs. Few studies have identified the number of mitochondria in NPCs. Morphological measurements of mitochondria did not reveal any differences between all genotypes analyzed, suggesting that fission and fusion dynamics may not contribute to the increased number of mitochondria observed in response to loss of Mcl-1. This is in contrast to the findings in cardiomyocytes where ablation of Mcl-1 resulted in abnormal mitochondrial ultrastructure, such as fragmented or degraded cristae structure and the formation of large vacuoles (Wang et al., 2014). Rather in NPCs, processes such as mitochondrial biogenesis, in which new mitochondria are created from the existing mitochondrial network, could potentially account for the increased number of mitochondria observed in response to loss of Mcl-1. However, the current assessment occurred in a 2D plane and may not fully represent the mitochondrial network at this timepoint. The findings of this thesis are unique as they demonstrate that this increase in mitochondria per NPCs was observed at the onset of neurogenesis; however, the E11 timepoint was only examined in this thesis. Mitochondrial number, morphology and biogenesis should therefore be examined prior to the onset of neurogenesis to determine the exact timepoint of these alterations. Mitochondrial function and morphological changes occur at the onset of

differentiation and are a necessary and vital process during neurogenesis (Homem et al., 2014; Stoll et al., 2015). The increase in mitochondrial number observed in MKOs at the onset of neurogenesis could therefore promote premature cell cycle exit and subsequent differentiation of NPCs. Ultimately, this thesis demonstrate a novel role of Mcl-1 in mediating mitochondrial number during neurogenesis.

4.3 Co-deletion of Mcl-1 and Bax rescues premature cell cycle exit and mitochondrial number

The results of this thesis demonstrate that the premature cell cycle exit of NPCs and increased number of mitochondria observed in response to loss of Mcl-1 is rescued in MKO: BaxKO embryos. Importantly, NPCs in Bax Null mice displayed no alterations in cell cycle exit and had comparable mitochondria numbers to control littermates. These results suggest that the removal of Bax expression at this time point does not affect cell cycle exit or mitochondrial numbers in NPCs. Bax is the dominant pro-apoptotic protein expressed during nervous system development (Krajewski et al., 2014). Furthermore, Bax is the primary pro-apoptotic target of Mcl-1 during developmental neurogenesis (Flemmer et al., 2021; Fogarty et al., 2019). The results of this thesis demonstrate a potential mechanism in which Mcl-1 prevents premature cell cycle exit and subsequent apoptosis, as well as regulating mitochondria number through inhibition of Bax. However, the nature of this interaction remains unclear. Like Mcl-1, recent studies have demonstrated the involvement of Bax in mitochondrial fission and fusion dynamics through its interaction with Drp-1 and MFN1 and MFN2 respectively (Brooks et al., 2007; Delivani et al., 2006; Hoppins et al., 2011). Whether Mcl-1 exerts its pro-survival function during developmental neurogenesis

through inhibiting the action of Bax in mitochondrial fission currently remains elusive and requires further investigation. As the size of mitochondria were comparable amongst all genotypes, this interaction could possibly be linked to processes such as mitochondrial biogenesis. Further investigation into the nature of the interaction of Mcl-1 and Bax in regards to cell cycle exit and mitochondrial number is necessary.

4.4 Validation of Nestin/Tom20 IHC with NanoJ SRRF processing as a method to quantify mitochondrial number and morphology

Mitochondrial number and morphology have commonly been measured through both fluorescence microscopy and EM analysis. Fluorescence microscopy is used to measure mitochondrial number and distribution (Chang et al., 2006; Takihara et al., 2015). EM analysis to examine mitochondrial morphology, size and structure is considered the gold standard for clinical analysis (Revishchin and Garey, 1996; Sakata and Jones, 2003). This thesis measured mitochondria in NPCs using Nestin/Tom20 IHC with NanoJ SRRF processing. SRRF processing produces super-resolution images for tissue labeled with conventional fluorophores and was used in this study to measure mitochondria in NPCs. To the best of our knowledge, IHC with NanoJ SRRF processing has not been used to measure mitochondria number and morphology and therefore is a novel technique for this application. In order to validate the results of this analysis, mitochondrial size and morphology were measured using EM analysis. The results obtained from the Nestin/Tom20 IHC with NanoJ SRRF processing analysis were comparable to the results obtained from EM analysis. Specifically, the values for the number of mitochondria and mitochondrial morphology were comparable in both analyses. This finding demonstrates the

use of Nestin/Tom20 IHC with NanoJ SRRF processing as a novel technique to measure mitochondrial number and morphology.

4.5 Future Directions

The results of this thesis demonstrate that there is an increase in mitochondria in the Mcl-1 CKO NPCs at the onset of neurogenesis. Though previous studies have demonstrated that Mcl-1 is expressed at the onset of neurogenesis (Fogarty et al., 2019), it is currently unknown if the increase in mitochondria in MKO NPCs is a result of loss of Mcl-1^{OM} or Mcl-1^{Matrix} or both. In order to examine the respective roles of Mcl-1^{OM} and Mcl-1^{Matrix} during neurogenesis, future experiments could conditionally knock-out each isoform in NPCs *in vitro.*

This study assessed mitochondrial morphology through both Nestin/Tom20 immunohistochemistry with NanoJ SRRF processing and through EM analysis. Ultrastructural analysis through scanning electron microscopy or three-dimensional reconstruction of mitochondrial networks through transmission electron microscopy would determine the effect of loss of Mcl-1 on mitochondrial morphology and mitochondrial networks at the onset of neurogenesis. Furthermore, the mechanism by which Mcl-1 maintains mitochondrial size at the onset of neurogenesis is currently unknown. Mcl-1 interacts with known fission/fusion proteins Drp1 and Opa1, with inhibition or silencing of the expression of Mcl-1 resulting in alterations to the mitochondrial networks (Rasmussen et al., 2018). Co-immunoprecipitation of Mcl-1 with known fission or fusion proteins would determine if Mcl-1 is regulating mitochondrial number through fission/fusion dynamics. As mitochondrial size was comparable across all genotypes analyzed, this could suggest that Mcl-1 mediates mitochondrial number through an alternate process such as mitochondrial

biogenesis. Future studies are necessary to determine if Mcl-1 mediates mitochondrial number through mitochondrial biogenesis at the onset of neurogenesis.

Neurogenesis is marked by a metabolic switch from glycolysis to OXPHOS, therefore determining the effect of loss of Mcl-1 on metabolism through measuring the rates of glycolysis and OXPHOS at the onset of neurogenesis is essential. As mitochondrial function and morphology mediate NPCs differentiation through modifying ROS signaling during neurogenesis (Khacho et al., 2016). Therefore, the impact of loss of Mcl-1 on ROS production at the onset of neurogenesis should be examined in the future.

The sex of the embryos was included in the descriptive data points for all experiments. Although there were insufficient samples from male and female tissue for statistical analysis, the data points appeared comparable for all experiments. In future, the number of male and female samples would need to be increased to determine the impact of sex on the obtained results.

4.6 Conclusion

This thesis examined the role of Mcl-1 in developmental neurogenesis. Loss of Mcl-1 results in premature cell cycle exit in the developing forebrain at the onset of neurogenesis. The rates of cell cycle exit differ between the MGE and dorsal cortex, with a greater amount of cell cycle exit occurring in the MGE at the onset of neurogenesis. Premature cell cycle exit in both regions resulted in apoptosis. Analysis of mitochondrial number and morphology using Nestin/Tom20 IHC with NanoJ SRRF processing and EM analysis revealed a significantly greater number of mitochondria in MKO NPCs at the onset of

neurogenesis, with no morphological changes. This thesis also validated the use of Nestin/Tom20 IHC with NanoJ SRRF processing as a novel method to examine mitochondria number and morphology. The observed phenotypes of MKOs were rescued in MKO: BaxKO embryos, indicating that an interaction between Mcl-1 and Bax is responsible for the observed phenotype. The findings of this thesis demonstrate a novel role of Mcl-1 in regulating cell cycle exit and mitochondrial number at the onset of developmental neurogenesis.

References

Abe-Dohmae S., Harada N., Yamada K., & Tanaka R. (1993). Bcl-2 gene is highly expressed during neurogenesis in the central nervous system. *Biochem. Biophys. Res. Commun*. 191, 915–92. DOI: 10.1006/bbrc.1993.1304.

Adams K. W., Cooper G. M. (2007). Rapid turnover of mcl-1 couples translation to cell survival and apoptosis. *J Biol. Chem.*, 282, 6192–6200. DOI: 10.1074/jcb.M610643200.

Agathocleous, M., Love, N., Randlett, O., Harris, J., Liu, J., Murray, A., & Harris, W. (2012). Metabolic differentiation in the embryonic retina. *Nat. Cell Biol.*, *14*(8), 859-864. DOI: 10.1038/ncb2531.

Alavian K. N., Li H., Collis L., Bonanni L., Zeng L., Sacchetti S., et al. (2011) Bcl-xL regulates metabolic efficiency of neurons through interaction with the mitochondrial F1FO ATP synthase. *Nat. Cell Biol*. 13, 1224–1233. DOI: 10.1038/ncb2330.

Alle, H., Roth, A., & Geiger, J. (2009). Energy-efficient action potentials in hippocampal mossy fibers. *E-Neuroforum*, *15*(4), 130-131. DOI: 10.1515/nf-2009-0405.

Altman, J., & Das, G. (1965). Autoradiographic and histological evidence of postnatal hippocampal neurogenesis in rats. *J. Comp. Neurol. 124*(3), 319-335. DOI: 10.1002/cne.901240303.

Angevine, J.B. & Sidman, R.L. (1961). Autoradiographic study of cell migration during histogenesis of cerebral cortex in the mouse. *Nature*, 192, 921-927. DOI: 10.1038/192766b0.

Anilkumar, U., Khacho, M., Cuillerier, A., Harris, R., Patten, D., & Bilen, M. (2020). MCL-1Matrix maintains neuronal survival by enhancing mitochondrial integrity and bioenergetic capacity under stress conditions. *Cell Death Dis.*, *11*(5). DOI: 10.1038/s41419-020-2498-9.

Anilkumar, U., & Prehn, J. H. M. (2014). Anti-apoptotic BCL-2 family proteins in acute neural injury. In *Front. Cell Neurosci.*, 8. DOI: 10.3389/fncel.2014.00281.

Annis R. P., Swahari V., Nakamura A., Xie A. X., Hammond S. M., Deshmukh M. (2016). Mature neurons dynamically restrict apoptosis via redundant premitochondrial brakes. *FEBS J,* 283, 4569–4582. DOI: 10.1111/febs.13944.

Anthony, T., Klein, C., Fishell, G., & Heintz, N. (2004). Radial glia serve as neuronal progenitors in all regions of the central nervous system. *Neuron*, *41*(6), 881-890. DOI: 10.1016/s0896-6273(04)00140-0.

Arbour, N., Vanderluit., J.L., Le Grand, J.N., Jahani-Asl, A., Ruzhynsky, V.A., Cheung, E.C.C., et al. (2008). Mcl-1 is a key regulator of apoptosis during CNS development and after DNA damage. *J Neurosci,* 28, 6068-78. DOI: 10.1523/JNeurosci.4940-07.2008.

Ashkenazi, A., Fairbrother, W. J., Leverson, J. D., & Souers, A. J. (2017). From basic apoptosis discoveries to advanced selective BCL-2 family inhibitors. In *Nat. Rev. Drug Discov*, 16(4), 273–284. Nature Publishing Group. DOI: 10.1038/nrd.2016.253.

Beckervordersandforth, R., Ebert, B., Schäffner, I., Moss, J., Fiebig, C., Shin, J., et al. (2017). Role of mitochondrial metabolism in the control of early lineage progression and aging phenotypes in adult hippocampal neurogenesis. *Neuron*, *93*(3), 560-573.e6. DOI: 10.1016/j.neuron.2016.12.017.

Bérubé, N., Mangelsdorf, M., Jagla, M., Vanderluit, J., Garrick, D., Gibbons, R. et al. (2005). The chromatin-remodeling protein ATRX is critical for neuronal survival during corticogenesis. *J. Clin Invest.*, *115*(2), 258-267. DOI: 10.1172/jci200522329.

Billen, L., Shamas-Din, A., & Andrews, D. (2008). Bid: a Bax-like BH3 protein. *Oncogene*, *27*(S1), S93-S104. DOI: 10.1038/onc.2009.47.

Brunelle, J., & Letai, A. (2009). Control of mitochondrial apoptosis by the Bcl-2 family. *J Cell Sci.*, *122*(4), 437-441. DOI: 10.1242/jcs.031682.

Bleicken, S., Hofhaus, G., Ugarte-Uribe, B., Schröder, R., & García-Sáez, A. (2016). cBid, Bax and Bcl-xL exhibit opposite membrane remodeling activities. *Cell Death Dis.*, *7*(2), e2121-e2121. DOI: 10.1038/cddis.2016.34.

Bouillet, P., Metcalf, D., Huang, D., Tarlinton, D., Kay, T., Köntgen, F. et al. (1999). Proapoptotic Bcl-2 relative bim required for certain apoptotic responses, leukocyte homeostasis, and to preclude autoimmunity. *Science*, *286*(5445), 1735-1738. DOI: 10.1126/science.286.5445.1735.

Burek, M., & Oppenheim, R. (1996). Programmed cell death in the developing nervous system. *Brain Pathol.*, *6*(4), 427-446. DOI: 10.1111/j.1750-3639.1996.tb00874.x.

Bursch, W., Paffe, S., Putz, B., Barthel, G., & Schulte-Hermann, R. (1990). Determination of the length of the histological stages of apoptosis in normal liver and in altered hepatic foci of rats. *Carcinogenesis*, *11*(5), 847-853. doi: 10.1093/carcin/11.5.847Cadwell, C. R., Bhaduri, A., Mostajo-Radji, M. A., Keefe, M. G., & Nowakowski, T. J. (2019). Development and Arealization of the Cerebral Cortex. *Neuron*, 103 (6), pp. 980–1004). DOI: 10.1016/j.neuron.2019.07.009.

Chang DT, Honick AS, Reynolds IJ. (2006). Mitochondrial trafficking to synapses in cultured primary cortical neurons. *J Neurosci*., 26, 7035–7045. DOI: 10.1523/JNeurosci.1012-06.2006.

Chipuk, J., Bouchier-Hayes, L., & Green, D. (2006). Mitochondrial outer membrane permeabilization during apoptosis: the innocent bystander scenario. *Cell Death Differ.*, *13*(8), 1396-1402. DOI:10.1038/sj.cdd.4401963.

Chen, S., Dai, Y., Harada, H., Dent, P., & Grant, S. (2007). Mcl-1 down-regulation potentiates ABT-737 lethality by cooperatively inducing Bak activation and Bax translocation. *Cancer Res.*, *67*(2), 782-791. DOI: 10.1158/0008-5472.can-06-3964.

Chen L., Willis S. N., Wei A., Smith B. J., Fletcher J. I., Hinds M. G., et al. (2005). Differential targeting of prosurvival Bcl-2 proteins by their BH3-only ligands allows complementary apoptotic function. *Mol. Cell*, 17, 393–403. DOI: 10.1016/j.molcel.2004.12.030.

Chen Y.-B., Aon M. A., Hsu Y.-T., Soane L., Teng X., McCaffery J. M., et al. (2011) Bcl-xL regulates mitochondrial energetics by stabilizing the inner membrane potential. *J. Cell Biol*. 195, 263–276. DOI: 10.1083/jcb.201108059.

Cheng E.H., Wei M.C., Weiler S., Flavell R.A., Mak T.W., Lindsten T., et al. (2001). BCL-2, BCL-x_L sequester BH3 domain-only molecules preventing BAX- and BAK-mediated mitochondrial apoptosis. *Mol Cell*, 8, 705–711. DOI: 10.1016/s1097-2765(01)00320-3.

Clarke, P.G., Posada, A., Primi, M.P., & Castagne., V. (1998). Neuronal death in the central nervous system during development. *Biomed Pharmacother, 52.* 356-362. DOI: 10.1016/S0753-3322(99)80002-X.

Cory, S., & Adams, J. (2002). The Bcl2 family: regulators of the cellular life-or-death switch. *Nat Rev Cancer*, *2*(9), 647-656. DOI: 10.1038/nrc883.

Cosulich, S., Worrall, V., Hedge, P., Green, S., & Clarke, P. (1997). Regulation of apoptosis by BH3 domains in a cell-free system. *Curr Biol.*, *7*(12), 913-920. DOI: 10.1016/s0960-9822(06)00410-6.

Dagda, R., Cherra, S., Kulich, S., Tandon, A., Park, D., & Chu, C. (2009). Loss of PINK1 function promotes mitophagy through effects on oxidative stress and mitochondrial fission. *J Biol Chem.*, *284*(20), 13843-13855. DOI: 10.1074/jbc.m808515200.

D'Arcy, M. S. (2019). Cell death: a review of the major forms of apoptosis, necrosis and autophagy. In *Cell Biol Int.* (Vol. 43, Issue 6, pp. 582–592). Wiley-Blackwell Publishing Ltd. DOI: 10.1002/cbin.11137.

Deckwerth, T., Elliott, J., Knudson, C., Johnson, E., Snider, W., & Korsmeyer, S. (1996). BAX is required for neuronal death after trophic factor deprivation and during Development. *Neuron*, *17*(3), 401-411. DOI: 10.1016/s0896-6273(00)80173-7.

Dekkers, M., Nikoletopoulou, V., & Barde, Y. (2013). Death of developing neurons: New insights and implications for connectivity. *J Cell Biol.*, *203*(3), 385-393. DOI: 10.1083/jcb.201306136.

Deng, J., Carlson, N., Takeyama, K., Dal Cin, P., Shipp, M., & Letai, A. (2007). BH3 profiling identifies three distinct classes of apoptotic blocks to predict response to ABT-737 and conventional chemotherapeutic agents. *Cancer Cell*, *12*(2), 171-185. DOI: 10.1016/j.ccr.2007.07.001.

Depaepe, V., Suarez-Gonzales, N., Dufour, A., Passante, L., Gorski, J.A., et al. (2005). Ephrin signalling controls brain size by regulating apoptosis of neural progenitors. *Nature*, 435, 1244-1250. DOI: 10.1038/nature03651.

Duan, C., Kuang, L., Hong, C., Xiang, X., Liu, J., Li, Q. et al. (2021). Mitochondrial Drp1 recognizes and induces excessive mPTP opening after hypoxia through BAX-PiC and LRRK2-HK2. *Cell Death Dis.*, *12*(11). DOI: 10.1038/s41419-021-04343-x.

Engel, T., Plesnila, N., Prehn, J., & Henshall, D. (2011). *In vivo* contributions of BH3-Only proteins to neuronal death following seizures, ischemia, and traumatic brain injury. *J Cereb Blood Flow Metab.*, *31*(5), 1196-1210. DOI: 10.1038/jcbfm.2011.26.

Fietz, S. A., & Huttner, W. B. (2011). Cortical progenitor expansion, self-renewal and neurogenesis-a polarized perspective. In *Current Opin Neurobiol.* (Vol. 21, Issue 1, pp. 23–35). DOI: 10.1016/j.conb.2010.10.002.

Finlay, B.L., & Pallas, S.L. (1989). Control of cell number in the developing mammalian visual system. *Prog Neurobiol*, 32, 207-234. DOI: 10.1016/0301-0082(89)90017-8.

Flemmer, R., Connolly, S., Geizer, B., Opferman, J., & Vanderluit, J. (2021). The role of Mcl-1 in embryonic neural precursor cell apoptosis. *Front Cell Dev Biol.*, 9. DOI: 10.3389/fcell/2021/659531.

Fogarty, L.C., Flemmer, R.T., Geizer, B.A., Licursi, M., Karunanithy, A., Opferman, J.T., et al. (2019). Mcl-1 and Bcl-xL are essential for survival of the developing nervous system. *Cell Death Differ.,* 26**,** 1501-1515. DOI: 10.1038/s41418-018-0225-1.

Fogarty, L., Song, B., Suppiah, Y., Hasan, S., Martin, H., & Hogan, S. et al. (2016). Bcl-xL dependency coincides with the onset of neurogenesis in the developing mammalian spinal cord. *Mol Cell Neurosci.*, *77*, 34-46. DOI: 10.1016/j.mcn.2016.09.001.

Götz, M., & Huttner, W. B. (2005). The cell biology of neurogenesis. In *Nat Rev Mol Cell Biol.* (Vol. 6, Issue 10, pp. 777–788). DOI: 10.1038/nrm1739.

Götz, M., Nakafuku, M., & Petrik, D. (2016). Neurogenesis in the developing and adult brain—similarities and key differences. *Cold Spring Harb Perspect Biol.*, *8*(7). DOI: 10.1101/cshperspect.a018853.

Germain M., Nguyen A. P., Le Grand J. N., Arbour N., Vanderluit J. L., Park D. S., et al. (2011). MCL-1 is a stress sensor that regulates autophagy in a developmentally regulated manner. *EMBO J, 30*, 395–407. DOI: 10.1038/emboj.2010.327.

Gouti M., Metzis V., Briscoe J. (2015). The route to spinal cord cell types: a tale of signals and switches. *Trends Genet.* 31, 282–289. DOI: 10.1016/j.tig.2015.03.001.

Hall, C., Klein-Flugge, M., Howarth, C., & Attwell, D. (2012). Oxidative phosphorylation, not glycolysis, powers presynaptic and postsynaptic mechanisms underlying brain information processing. *J Neurosci.*, *32*(26), 8940-8951. DOI: 10.1523/jneurosci.0026-12.2012.

Hamburger V., Brunso-Bechtold J.K., & Yip J.W. (1981). Neuronal death in the spinal ganglia of the chick embryo and its reduction by nerve growth factor. *J. Neurosci,* 1, 60–71. DOI: 10.1523/JNeurosci.01-01-00060.1981.

Hardwick, J., & Soane, L. (2013). Multiple functions of BCL-2 family proteins. *Cold Spring Harb Perspect Biol.*, *5*(2). DOI: 10.1101/cshperspect.a008722.

Harley M. E., Allan L. A., Sanderson H. S., Clarke P. R. (2010). Phosphorylation of Mcl-1 by CDK1-cyclin B1 initiates its Cdc20-dependent destruction during mitotic arrest. *EMBO J,* 29, 2407–2420. DOI: 10.1038/emboj.2010.112.

Hasan, S.M., Sheen., A.D., Power, A.M., Langevin, L.M., Xiong, J., Furlong, M., Day, K., et al. (2013). Mcl1 regulates the terminal mitosis of neural precursor cells in the mammalian brain through p27Kip1. *Development,* 140, 3118-27. DOI: 10.1242/dev.090910.

Haubensak, W., Attardo, A., Denk, W., & Huttner, W. (2004). Neurons arise in the basal neuroepithelium of the early mammalian telencephalon: A major site of neurogenesis. *Proc Natl Acad Sci USA., 101*(9), 3196-3201. DOI: 10.1073/pnas.0308600100.

Haydar, T.F., Kuan, C.Y., Flavell., R.A., Rakic, P. (1999). The role of cell death in regulating the size and shape of the mammalian forebrain. *Cereb Cortex,* 9, 621-626. DOI: 10.1093/cercor/9.6.621.

Henshall, D. C., & Engel, T. (2013). Contribution of apoptosis-associated signaling pathways to epileptogenesis: Lessons from Bcl-2 family knockouts. *Front Cell Neurosci.*, 7(1), 110. DOI: 10.3389/fncel.2013.00110.

Hjelm, B., Rollins, B., Mamdani, F., Lauterborn, J., Kirov, G., & Lynch, G. (2015). Evidence of mitochondrial dysfunction within the complex genetic etiology of schizophrenia. *Mol Neuropsychiatry.*, *1*(4), 201-219. DOI: 10.1159/000441252.

Hollville, E., Romero, S. E., & Deshmukh, M. (2019). Apoptotic cell death regulation in neurons. In *FEBS Journal*, 286 (17), 3276–3298. Blackwell Publishing Ltd. DOI: 10.1111/febs.14970.

Homem, C. C. F., Steinmann, V., Burkard, T. R., Jais, A., Esterbauer, H., & Knoblich, J. A. (2014). Ecdysone and mediator change energy metabolism to terminate proliferation in drosophila neural stem cells. *Cell*, *158*(4), 874–888. DOI: 10.1016/j.cell.2014.06.024.

Hoppins, S., Edlich, F., Cleland, M., Banerjee, S., McCaffery, J., Youle, R., et al. (2011). The soluble form of Bax regulates mitochondrial fusion via MFN2 homotypic complexes. *Mol Cell*, *41*(2), 150-160. DOI: 10.1016/j.molcel.2010.11.030.

Hu, C., Fan, L., Cen, P., Chen, E., Jiang, Z., & Li, L. (2016). Energy metabolism plays a critical role in stem cell maintenance and differentiation. In *Int J Mol Sci.*, 17(2), 253. DOI: 10.3390/ijms17020253.

Huang, D., & Strasser, A. (2000). BH3-Only proteins—essential initiators of apoptotic cell death. *Cell*, *103*(6), 839-842. DOI: 10.1016/s0092-8674(00)00187-2.

Huang, H., Hu, X., Eno, C., Zhao, G., Li, C., & White, C. (2013). An interaction between Bcl-xL and the voltage-dependent anion channel (VDAC) promotes mitochondrial Ca2+ uptake. *J BiolChem.*, *288*(27), 19870-19881. DOI: 10.1074/jbc.m112.448290.

Huttner, W., & Brand, M. (1997). Asymmetric division and polarity of neuroepithelial cells. *Curr Opin Neurobiol.*, *7*(1), 29-39. DOI: 10.1016/s0959-4388(97)80117-.

Iwata, R., Casimir, P., & Vanderhaeghen, P. (2020). Mitochondrial dynamics in postmitotic cells regulate neurogenesis. *Science*, *369*(6505), 858-862. doi: 10.1126/science.aba9760.

Jin, X. (2016). The role of neurogenesis during development and in the adult brain. *Euro J Neurosci.*, *44*(6), 2291-2299. DOI: 10.1111/ejn.13251.

Joshi, P., Bodnya, C., Rasmussen, M., Romero-Morales, A., Bright, A., & Gama, V. (2020). Modeling the function of BAX and BAK in early human brain development using iPSC-derived systems. *Cell Death Dis.*, *11*(9). DOI: 10.1038/s41419-020-03002-x.

Jürgensmeier, J., Xie, Z., Deveraux, Q., Ellerby, L., Bredesen, D., & Reed, J. (1998). Bax directly induces release of cytochrome c from isolated mitochondria. *Proc Natl Acad Sci USA.*, *95*(9), 4997-5002. DOI: 10.1073/pnas.95.9.4997.

Karbowski, M., Lee, Y., Gaume, B., Jeong, S., Frank, S., & Nechushtan, A. et al. (2002). Spatial and temporal association of Bax with mitochondrial fission sites, Drp1, and Mfn2 during apoptosis. *J Cell Biol.*, *159*(6), 931-938. DOI: 10.1083/jcb.200209124.

Kerr, J., Wyllie, A., & Currie, A. (1972). Apoptosis: a basic biological phenomenon with wideranging implications in tissue kinetics. *Br J Cancer*, *26*(4), 239-257. DOI: 10.1038/bjc.1972.33.

Khacho, M., Clark, A., Svoboda, D. S., Azzi, J., MacLaurin, J. G., Meghaizel, C., Sesaki, H., et al. (2016). Mitochondrial dynamics impacts stem cell identity and fate decisions by regulating a nuclear transcriptional program. *Cell Stem Cell*, *19*(2), 232–247. DOI: 10.1016/j.stem.2016.04.015.

Khacho, M., Clark, A., Svoboda, D. S., MacLaurin, J. G., Lagace, D. C., Park, D. S., & Slack, R. S. (2017). Mitochondrial dysfunction underlies cognitive defects as a result of neural stem cell depletion and impaired neurogenesis. *Human Mol Gene.*, *26*(17), 3327–3341. DOI: 10.1093/hmg/ddx217.

Khacho, M., Harris, R., & Slack, R. S. (2019). Mitochondria as central regulators of neural stem cell fate and cognitive function. *Nat Rev Neurosci* (Vol. 20, Issue 1, pp. 34–48). Nature Publishing Group. DOI: 10.1038/s41583-018-0091-3.

Kluck, R., Esposti, M., Perkins, G., Renken, C., Kuwana, T., Bossy-Wetzel, E. et al. (1999). The pro-apoptotic proteins, Bid and Bax, cause a limited permeabilization of the mitochondrial outer membrane that is enhanced by cytosol. *J Cell Biol.*, *147*(4), 809-822. DOI: 10.1083/jcb.147.4.809.

Knudson C. M., Tung K. S., Tourtellotte W. G., Brown G. A., & Korsmeyer S. J. (1995). Bax-deficient mice with lymphoid hyperplasia and male germ cell death. *Science*, 270, 96–99. DOI: 10.1126/science.270.5233.96.

Kole, A., Annis, R., & Deshmukh, M. (2013). Mature neurons: equipped for survival. *Cell Death Dis.*, *4*(6), e689-e689. DOI: 10.1038/cddis.2013.220.

Kozopas K. M., Yang T., Buchan H. L., Zhou P., Craig R. W. (1993). MCL1, a gene expressed in programmed myeloid cell differentiation, has sequence similarity to BCL2. *Proc. Natl. Acad. Sci. U.S.A,* 90, 3516–3520. DOI: 10.1073/pnas.90.8.3516.

Krajewska, M., Mai, J., Zapata, J., Ashwell, K., Schendel, S., Reed, J., et al. (2002). Dynamics of expression of apoptosis-regulatory proteins Bid, Bcl-2, Bcl-X, Bax and Bak during development of murine nervous system. *Cell Death Differ.*, *9*(2), 145-157. DOI: 10.1038/sj.cdd.4400934.

Kristiansen, M., & Ham, J. (2014). Programmed cell death during neuronal development: The sympathetic neuron model. In *Cell Death & Differ.* (Vol. 21, Issue 7, pp. 1025–1035). DOI: 10.1038/cdd.2014.47.

Kuan, C.Y., Roth, K.A., Flavell, R.A., Rakic, P. (2000). Mechanisms of programmed cell death in the developing brain. *Trends Neurosci.*, 23, 291-297. DOI: 10.1016/s0166-2236(00)01581-2.

Lindsten, T., Ross, A., King, A., Zong, W., Rathmell, J., & Shiels, H. (2000). The combined functions of proapoptotic Bcl-2 family members Bak and Bax Are essential for normal development of multiple tissues. *Mol Cell*, *6*(6), 1389-1399. DOI: 10.1016/s1097-2765(00)00136-2.

Liu, X., Kim, C., Yang, J., Jemmerson, R., & Wang, X. (1996). Induction of apoptotic program in cell-free extracts: requirement for dATP and cytochrome c. *Cell*, *86*(1), 147-157. DOI: 10.1016/s0092-8674(00)80085-9.

Liu, X., Zou, H., Slaughter, C., & Wang, X. (1997). DFF, a heterodimeric protein that functions downstream of caspase-3 to trigger DNA fragmentation during apoptosis. *Cell*, *89*(2), 175-184. DOI: 10.1016/s0092-8674(00)80197-x.

Llorens-Bobadilla, E., Zhao, S., Baser, A., Saiz-Castro, G., Zwadlo, K., & Martin-Villalba, A. (2015). Single-cell transcriptomics reveals a population of dormant neural stem cells that become activated upon brain injury. *Cell Stem Cell*, *17*(3), 329–340. DOI: 10.1016/j.stem.2015.07.002.

Maes, M., Grosser, J., Fehrman, R., Schlamp, C., & Nickells, R. (2019). Completion of BAX recruitment correlates with mitochondrial fission during apoptosis. *Sci.Rep.*, *9*(1). DOI: 10.1038/s41598-019-53049-w.

McDonnell, T., Deane, N., Platt, F., Nunez, G., Jaeger, U., McKearn, J., & Korsmeyer, S. (1989). Bcl-2-Immunoglobulin transgenic mice demonstrate extended B cell survival and follicular lymphoproliferation. *Cell*, *57*(1), 79-88. DOI: 10.1016/0092-8674(89)90174-8.

Mei, Y., Xie, C., Xie, W., Tian, X., Li, M., & Wu, M. (2007). Noxa/Mcl-1 balance regulates susceptibility of cells to camptothecin-induced apoptosis. *Neoplasia*, *9*(10), 871-881. DOI: 10.1593/neo.07589.

Merry D. E., Veis D. J., Hickey W. F., & Korsmeyer S. J. (1994). bcl-2 protein expression is widespread in the developing nervous system and retained in the adult PNS. *Development*, 120, 301–311. DOI: 10.1242/dev.120.2.301.

Michaelidis, T., Sendtner, M., Cooper, J., Airaksinen, M., Holtmann, B., Meyer, M., et al. (1996). Inactivation of bcl-2 results in progressive degeneration of motoneurons, sympathetic and sensory neurons during early postnatal development. *Neuron*, *17*(1), 75-89. DOI: 10.1016/s0896-6273(00)80282-2.

Miyata, T., Kawaguchi, A., Okano, H., & Ogawa, M. (2001). Asymmetric inheritance of radial glial fibers by cortical neurons. *Neuron*, *31*(5), 727-741. DOI: 10.1016/s0896-6273(01)00420-2.

Molnár, Z., Vasistha, N., & Garcia-Moreno, F., (2011). Hanging by the tail; progenitor populations proliferate. *Nat Neurosci.,* 14(5), 538-40. DOI: 10.1038/nn.2817.

Motoyama, N., Wang, F., Roth, K., Sawa, H., Nakayama, K., & Nakayama, K. et al. (1995). Massive cell death of immature hematopoietic cells and neurons in Bcl-x-deficient mice. *Science*, *267*(5203), 1506-1510. DOI: 10.1126/science.7878471.

Nakamura, A., Swahari, V., Plestant, C., Smith, I., McCoy, E., Smith, S., Moy, S.S., Anton, E.S., Deshmukh, M. (2016). Bcl-xL is essential for the survival and function of differentiated neurons in the cortex that control complex behaviours. *J Neurosci.,* 36, 5448-5461. DOI: 10.1523/JNeurosci.4247-15.2016.

Noctor, S., Flint, A., Weissman, T., Dammerman, R., & Kriegstein, A. (2001). Neurons derived from radial glial cells establish radial units in neocortex. *Nature*, *409*(6821), 714-720. DOI: 10.1038/35055553.

Nornes, H. & Carry., M. (1978). Neurogenesis in spinal cord of mouse; an autoradiographic analysis. *Brain Res.,* 159, 1-6. DOI: 10.1016/0006-8993(78)90105-1.

Oltval, Z., Milliman, C., & Korsmeyer, S. (1993). Bcl-2 heterodimerizes in vivo with a conserved homolog, Bax, that accelerates programed cell death. *Cell*, *74*(4), 609-619. DOI: 10.1016/0092-8674(93)90509-o.

Opferman, J. T., & Kothari, A. (2018). Anti-apoptotic BCL-2 family members in development. In *Cell Death Differ.*, 25 (1), 37–45. Nature Publishing Group. DOI: 10.1038/cdd.2017.170.

Opferman J. T., Letai A., Beard C., Sorcinelli M. D., Ong C. C., Korsmeyer S. J. (2003). Development and maintenance of B and T lymphocytes requires antiapoptotic MCL-1. *Nature*, 426, 671–676. DOI: 10.1038/nature02067.

Oppenheim, R. (1991). Cell death during development of the nervous system. *Annu Rev Neurosci.*, *14*(1), 453-501. DOI: 10.1146/annurev.ne.14.030191.002321.

Perciavalle, R., Stewart, D., Koss, B., Lynch, J., Milasta, S., & Bathina, M. et al. (2012). Anti-apoptotic MCL-1 localizes to the mitochondrial matrix and couples mitochondrial fusion to respiration. *Nat Cell Biol.*, *14*(6), 575-583. DOI: 10.1038/ncb2488.

Petros, A., Nettesheim, D., Wang, Y., Olejnicazk, E., Meadows, R., & Mack, J. et al. (2000). Rationale for Bcl-xL/Bad peptide complex formation from structure, mutagenesis, and biophysical studies. *Protein Sci.*, *9*(12), 2528-2534. DOI: 10.1017/s096183680000331x.

Polster, B., Basañez, G., Young, M., Suzuki, M., & Fiskum, G. (2003). Inhibition of Bax-induced cytochrome c release from neural cell and brain mitochondria by dibucaine and propranolol. *J Neurosci.*, *23*(7), 2735-2743. DOI: 10.1523/jneurosci.23-07-02735.2003.

Print, C., Loveland, K., Gibson, L., Meehan, T., Stylianou, A., & Wreford, N. et al. (1998). Apoptosis regulator Bcl-w is essential for spermatogenesis but appears otherwise redundant. *Proc Natl Acad Sci USA.*, *95*(21), 12424-12431. DOI: 10.1073/pnas.95.21.12424.

Rajasekaran, A., Venkatasubramanian, G., Berk, M., & Debnath, M. (2015). Mitochondrial dysfunction in schizophrenia: Pathways, mechanisms and implications. *Neurosci Biobehav Rev.*, *48*, 10-21. DOI: 10.1016/j.neubiorev.2014.11.005.

Rakic, P. (1988). Specification of cerebral cortical areas. *Science*, *241*(4862), 170-176. DOI: 10.1126/science.3291116.

Rasmussen, M., Kline, L., Park, K., Ortolano, N., Romero-Morales, A., & Anthony, C. et al. (2018). A non-apoptotic function of MCL-1 in promoting pluripotency and modulating mitochondrial dynamics in stem cells. *Stem Cell Reports*, *10*(3), 684-692. DOI: 10.1016/j.stemcr.2018.01.005.

Revishchin AV, Garey LJ. (1996). Mitochondrial distribution in visual and auditory cerebral cortex of the harbour porpoise. *Brain Behav Evol*. 47:257–266. DOI: 10.1159/000113245.

Reynolds, B., & Weiss, S. (1992). Generation of neurons and astrocytes from isolated cells of the adult mammalian central nervous system. *Science*, *255*(5052), 1707-1710. DOI: 10.1126/science.1553558.

Rinkenberger, J., Horning, S., Klocke, B., Roth, K., & Korsmeyer, S. (2000). Mcl-1 deficiency results in peri-implantation embryonic lethality. *Genes Dev.*, *14*(1), 23-27. DOI: 10.1101/gad.14.1.23.

Ross, A., Waymire, K., Moss, J., Parlow, A., Skinner, M., Russell, L., & MacGregor, G. (1998). Testicular degeneration in Bclw-deficient mice. *Nature Genet.*, *18*(3), 251-256. DOI: 10.1038/ng0398-251.

Rossé, T., Olivier, R., Monney, L., Rager, M., Conus, S., & Fellay, I. et al. (1998). Bcl-2 prolongs cell survival after Bax-induced release of cytochrome c. *Nature*, *391*(6666), 496-499. DOI: 10.1038/35160.

Sakata JT, & Jones TA. (2003). Synaptic mitochondrial changes in the motor cortex following unilateral cortical lesions and motor skills training in adult male rats. *Neurosci Lett*. 337:159–162. DOI: 10.1016/S0304-3940(02)01328-9.

Savitt JM, Jang SS, Mu W, Dawson VL, Dawson TM. (2005). Bcl-x is required for proper development of the mouse substantia nigra. *J Neurosci*, 25. 6721–6728. DOI: 10.1523/JNeurosci.0760-05.2005.

Schenk, R., Tuzlak, S., Carrington, E., Zhan, Y., Heinzel, S., & Teh, C. et al. (2017). Characterisation of mice lacking all functional isoforms of the pro-survival BCL-2 family member A1 reveals minor defects in the haematopoietic compartment. *Cell Death Differ.*, *24*(3), 534-545. DOI: 10.1038/cdd.2016.156.

Shamas-Din, A., Brahmbhatt, H., Leber, B., & Andrews, D. (2011). BH3-only proteins: Orchestrators of apoptosis. *Biochim Biophys Acta (BBA) - Mol Cell Res*, *1813*(4), 508-520. DOI: 10.1016/j.bbamcr.2010.11.024.

Shibue, T., Takeda, K., Oda, E., Tanaka, H., Murasawa, H., & Takaoka, A. et al. (2003). Integral role of Noxa in p53-mediated apoptotic response. *Genes Devt*, *17*(18), 2233-2238. DOI: 10.1101/gad.1103603.

Shindler, K., Latham, C., & Roth, K. (1997). baxDeficiency Prevents the increased cell death of Immature neurons inbcl-x-Deficient Mice. *J Neurosci*, *17*(9), 3112-3119. DOI: 10.1523/jneurosci.17-09-03112.1997.

Stoll, E. A., Makin, R., Sweet, I. R., Trevelyan, A. J., Miwa, S., Horner, P. J., & Turnbull, D. M. (2015). Neural stem cells in the adult subventricular zone oxidize fatty acids to produce energy and support neurogenic activity. *Stem Cells*, *33*(7), 2306–2319. DOI: 10.1002/stem.2042.

Tait, S., & Green, D. (2010). Mitochondria and cell death: outer membrane permeabilization and beyond. *Nat Rev Mol Cell Biol*, *11*(9), 621-632. DOI: 10.1038/nrm2952.

Takihara Y, Inatani M, Eto K, Inoue T, Kreymerman A, Miyake S, et al. (2015). In vivo imaging of axonal transport of mitochondria in the diseased and aged mammalian CNS. *Proc Natl Acad Sci USA*. 112:10515–10520. DOI: 10.1073/pnas.1509879112.

Tsujimoto, Y., Jaffe, E., Cossman, J., Gorham, J., Nowell, P., & Croce, C. (1985). Clustering of breakpoints on chromosome 11 in human B-cell neoplasms with the t(11 ; 14) chromosome translocation. *Nature*, *315*(6017), 340-343. DOI: 10.1038/315340a0.

Yao, B., Christian, K. M., He, C., Jin, P., Ming, G. L., & Song, H. (2016). Epigenetic mechanisms in neurogenesis. In *Nat Rev Neurosci* (Vol. 17, Issue 9, pp. 537–549). DOI: 10.1038/nrn.2016.70.

Vander Heiden, M., Chandel, N., Williamson, E., Schumacker, P., & Thompson, C. (1997). Bcl-xL regulates the membrane potential and volume homeostasis of mitochondria. *Cell*, *91*(5), 627-637. DOI: 10.1016/s0092-8674(00)80450-x.

Vaux, D., Cory, S., & Adams, J. (1988). Bcl-2 gene promotes haemopoietic cell survival and cooperates with c-myc to immortalize pre-B cells. *Nature*, *335*(6189), 440-442. DOI: 10.1038/335440a0.

Veleta, K., Cleveland, A., Babcock, B., He, Y., Hwang, D., Sokolsky-Papkov, M., & Gershon, T. (2020). Antiapoptotic Bcl-2 family proteins BCL-xL and MCL-1 integrate neural progenitor survival and proliferation during postnatal cerebellar neurogenesis. *Cell Death Differ*, *28*(5), 1579-1592. DOI: 10.1038/s41418-020-00687-7.

Villunger, A., Michalak, E., Coultas, L., Müllauer, F., Böck, G., Ausserlechner, M. et al. (2003). p53- and drug-induced apoptotic responses mediated by BH3-Only proteins Puma and Noxa. *Science*, *302*(5647), 1036-1038. DOI: 10.1126/science.1090072.

Wang, X., Bathina, M., Lynch, J., Koss, B., Calabrese, C., Frase, S. et al. (2013). Deletion of MCL-1 causes lethal cardiac failure and mitochondrial dysfunction. *Genes Dev.*, *27*(12), 1351-1364. DOI: 10.1101/gad.215855.113.

Warr, M., Acoca, S., Liu, Z., Germain, M., Watson, M., Blanchette, M. et al. (2005). BH3-ligand regulates access of MCL-1 to its E3 ligase. *FEBS Letters*, *579*(25), 5603-5608. DOI: 10.1016/j.febslet.2005.09.028.

Wiemerslage, L., & Lee, D. (2016). Quantification of mitochondrial morphology in neurites of dopaminergic neurons using multiple parameters. *J Neurosci Methods*, *262*, 56-65. DOI: 10.1016/j.jneumeth.2016.01.008.

Willis, S., Chen, L., Dewson, G., Wei, A., Naik, E., & Fletcher, J. et al. (2005). Proapoptotic Bak is sequestered by Mcl-1 and Bcl-xL, but not Bcl-2, until displaced by BH3-only proteins. *Genes Dev.*, *19*(11), 1294-1305. DOI: 10.1101/gad.1304105.

Yang, T., Kozopas, K., & Craig, R. (1995). The intracellular distribution and pattern of expression of Mcl-1 overlap with, but are not identical to, those of Bcl-2. *J Cell Biol.*, *128*(6), 1173-1184. DOI: 10.1083/jcb.128.6.1173.

Youle, R., & Strasser, A. (2008). The BCL-2 protein family: opposing activities that mediate cell death. *Nat Rev Mol Cell Biol.*, *9*(1), 47-59. DOI: 10.1038/nrm2308.

Zheng, X., Boyer, L., Jin, M., Mertens, J., Kim, Y., & Ma, L. et al. (2016). Metabolic reprogramming during neuronal differentiation from aerobic glycolysis to neuronal oxidative phosphorylation. *Elife*, *5*. DOI: 10.7554/elife.13374.

Zhong, Q., Gao, W., Du, F., & Wang, X. (2005). Mule/ARF-BP1, a BH3-Only E3 ubiquitin ligase, catalyzes the polyubiquitination of Mcl-1 and regulates apoptosis. *Cell*, *121*(7), 1085-1095. DOI: 10.1016/j.cell.2005.06.009.

Zou, H., Henzel, W., Liu, X., Lutschg, A., & Wang, X. (1997). Apaf-1, a human protein homologous to C. elegans CED-4, participates in cytochrome c–dependent activation of caspase-3. *Cell*, *90*(3), 405-413. DOI: 10.1016/s0092-8674(00)80501-2.

Appendix

Vanderluit, Jacqueline

From: nfairbridge@mun.ca
Sent: Monday, August 14, 2017 2:54 PM
To: Dr. Jacqueline Vanderluit (Principal Investigator)
Cc: ors@mun.ca; nfairbridge@mun.ca
Subject: Your Animal Use Protocol has been renewed

Institutional Animal Care Committee (IACC)
St. John's, NL, Canada A1C 5S7
Tel: 709 777-6620 acs@mun.ca
www.mun.ca/research/about/acs/

Dear: Dr. Jacqueline Vanderluit, Associate Professor/Faculty of Medicine\Division of BioMedical Sciences

Researcher Portal File No.: 20180541
Animal Care File: 17-02-JV
Entitled: (17-02-JV) The role of Bcl-2 proteins in developmental neurogenesis.
Status: Active
Related Awards:
Approval Date: August 01, 2017
Annual Report Due: August 01, 2018
Ethics Clearance Expires: August 01, 2020

Awards File No	Title	Status	
20161829	The role of Bcl-2 family proteins in developmental neurogenesis	Active	RGCS/CCCS

Your Animal Use Protocol has been renewed for a three-year term. This file replaces previous Animal Care ID [14-02-JV] as the active ethics clearance associated with this project. Please note the new file ID and Animal Care ID when referring to this protocol.

1. The committee requests that the lay summary be simplified for future submissions. It is recommended to write the lay summary as if presenting work to those with a basic understanding of biological research.

An Event [Annual Report] will be required following each year of protocol activity.

Should you encounter an unexpected incident that negatively affects animal welfare or the research project relating to animal use, please submit an Event [Incident Report].

Any alterations to the protocol requires prior submission and approval of an Event [Amendment].

Sincerely,

Nicholas Fairbridge, PhD
ACC Coordinator
Animal Care Services

Vanderluit, Jacqueline

From: ambakwe@mun.ca
Sent: September 14, 2020 1:14 PM
To: Vanderluit Jacqueline(Principal Investigator)
Cc: ambakwe@mun.ca
Subject: Your Animal Use Protocol has been renewed

Animal Care Committee (ACC)
St. John's, NL, Canada A1C 5S7
Tel: 709 777-6620 acs@mun.ca
https://www.mun.ca/research/about/acs/acc/

Dear: Dr. Jacqueline Vanderluit, Faculty of Medicine\Division of BioMedical Sciences

Researcher Portal File No.: 20210614
Animal Care File: 20-02-JV
Entitled: (20-02-JV) The role of Bcl-2 proteins in developmental neurogenesis.
Status: Active
Related Awards:

Awards File No	Title	Status	
20161829	The role of Bcl-2 family proteins in developmental neurogenesis	Active	1. Research Grant and Contract Services (RGCS) – St. John's and Grenfell Campuses

Ethics Clearance Terminates: August 01, 2023

Your Animal Use Protocol has been renewed for a three-year term. This file replaces previous File ID [[20180541]] and Animal Care ID [[17-02-JV]] as the active ethics clearance associated with this project. Please note the new file ID and Animal Care ID when referring to this protocol.

This ethics clearance includes the following Team Members: Dr. Jacqueline Vanderluit (Principal Investigator)

This ethics clearance includes the following related awards:

Awards File No	Title	Status	
20161829	The role of Bcl-2 family proteins in developmental neurogenesis	Active	1. Research Grant and Contract Services (RGCS) – St. John's and Grenfell Campuses

An Event [Annual Report] will be required following each year of protocol activity.

Should you encounter an unexpected incident that negatively affects animal welfare or the research project relating to animal use, please submit an Event [Incident Report].

Any alterations to the protocol requires prior submission and approval of an Event [Amendment].

NOTE: You can access a copy of this email at any time under the "Shared Communications" section of the Logs tab of your file in the Memorial Researcher Portal.

Sincerely,

ANULIKA MBAKWE | ACC COORDINATOR
Department of Animal Care Services
Memorial University of Newfoundland
Health Sciences Centre | Room H1848
P: 709-777-6621
E-Mail: ambakwe@mun.ca